INFORMATION TO USERS

This manuscript has been reproduced from the microfilm master. UMI films the text directly from the original or copy submitted. Thus, some thesis and dissertation copies are in typewriter face, while others may be from any type of computer printer.

The quality of this reproduction is dependent upon the quality of the copy submitted. Broken or indistinct print, colored or poor quality illustrations and photographs, print bleedthrough, substandard margins, and improper alignment can adversely affect reproduction.

In the unlikely event that the author did not send UMI a complete manuscript and there are missing pages, these will be noted. Also, if unauthorized copyright material had to be removed, a note will indicate the deletion.

Oversize materials (e.g., maps, drawings, charts) are reproduced by sectioning the original, beginning at the upper left-hand corner and continuing from left to right in equal sections with small overlaps.

ProQuest Information and Learning
300 North Zeeb Road, Ann Arbor, MI 48106-1346 USA
800-521-0600

DIFFUSION AND FLOW OF GASES THROUGH POROUS MEDIA

by

K. P. Chu

A thesis submitted to the
Department of Chemical Engineering
of
The University of Ottawa
in partial fulfilment of the requirements
for the degree of M.Sc.

Thesis Author

Research Director

1963

TABLE OF CONTENTS

I - ABSTRACT

Diffusivities for the binary system of H_2 - N_2 and permeabilities of N_2 were measured for seven types of porous material over the pressure range 0.2 - 70 atm. These measurements were made in both axial and radial directions to investigate the isotropy of pore properties.

Diffusivities and permeabilities were related to pore size distribution determined independently by mercury penetration. The method of Wakao and Smith gave satisfactory agreement except for the Nickel Catalyst and Vycor glass. In addition, diffusivities and permeabilities were related to each other satisfactorily.

The relative contribution of macropores and micropores to diffusion at various pressures has been studied. The results for two different carbon pellets indicate that the micropores of these materials consist of largely blind pores. In the case of a Molybdena Alumina Catalyst, the entire micropore volume contributes to diffusion.

A pore model for Vycor glass has been proposed and the controlling pore radius for this material calculated from the measured diffusivities.

II - INTRODUCTION

The process of diffusion of gases in the pore channels or the internal void space of porous materials is of great significance in operations concerned with chemical reactions in catalyst beds, adsorption units and gaseous separation processes. Also, problems involving flow of fluids through porous media arise in many branches of chemical engineering and petroleum technology. General applications are filtration, flow through packed beds and the production of oil from underground reservoirs where oil flows through sandstone and limestone. The interpretation of reaction rates and transport properties of these processes require a knowledge of diffusivity and permeability of the porous materials.

For the design of high pressure catalytic reactors or adsorbers, in addition to diffusion coefficients, a knowledge of permeabilities is required because the latter becomes important at high pressures. (24).

Effective diffusivity D_{eff} and effective permeability K_{eff} can be obtained from diffusion and forced flow measurements, but it is desirable to relate these transport coefficients (D_{eff} and K_{eff}) to the internal pore structure because (1) it is of interest in reaction rate studies to know how the various pores contribute to the flow, particularly the micropores; and (2) it is convenient to predict D_{eff} from pore size distribution for materials which cannot be mounted for measurement because of small size or irregular shape.

The method of mercury penetration for obtaining pore size distribution accounts for the controlling pore radii only and includes the blind pores which take no part in the flow. It may therefore be impossible to predict diffusivity from pore size distribution alone. In such cases, it would be convenient to predict D_{eff} from permeability which is easier to

measure.

The objects of this study are therefore defined as follows:

(1) to measure diffusivity D_{eff} and permeability K_{eff} of various materials over a wide pressure range particularly to assess micropore contribution,

(2) to relate D_{eff} and K_{eff} to the internal pore structure, and

(3) to relate D_{eff} to K_{eff}.

III - THEORETICAL CONSIDERATIONS AND LITERATURE REVIEW

A. Diffusion of Gases in Porous Media

Diffusion is considered to be the process where the transport of gases results from a gradient in concentration.

A molecule of gas is imagined to travel in a straight line and in a certain direction at a uniform velocity until it collides with another molecule. Due to the intermolecular collision, the molecule travels a complex zig-zag path and the net distance it moves is thus reduced. It is expected that the rate of diffusion depends on the number of collisions per unit time and the velocity of the molecule. Intermolecular collision and the collision with pore wall are recognized to be the main resistances for the transport of gases in pores. The type of diffusion depends on the total pressure and the mean free path which is the average distance the gas molecule travels.

Two limiting conditions are recognized to describe the mechanism of gaseous diffusion. If the pore channel is small relative to the mean free path λ, molecules collide more frequently with the pore wall than with each other, then transport occurs by Knudsen flow. It is obvious that Knudsen diffusion is independent of the total pressure and viscosity, but depends on the pore radius. Bulk diffusion (i. e. ordinary diffusion) occurs when the mean free path λ is small relative to the pore channel, molecules within the pore will collide with other molecules far more often than with the pore wall. Thus, intermolecular collisions control the rate of transport. Ordinary diffusion is inversely proportional to the total pressure and does not depend on the pore radius.

If the conditions of diffusion are such that r has the same magnitude as λ, then the diffusion process will have a mixed character

which combines the Knudsen and bulk diffusion. For materials consisting of macropores and micropores, a plot of D_{eff} vs. P will generally show three types of diffusion: (1) the Knudsen diffusion at very low pressures (< 0.1 atm); (2) the mixed diffusion at intermediate pressures (0.1 - 5 atm); and (3) the bulk diffusion at rather high pressures (> 5 atm).

The rate of diffusion is governed by Fick's law which states that the species of a certain component diffuse through a binary mixture in the direction of decreasing mole fraction of that component. Fick's law in terms of the molar flux N_A is given (22) as:

$$N_A = -D \frac{P}{RT} \frac{dy}{dz} \qquad (1)$$

Equation (1) may be applied to diffusion through porous materials by replacing D with an effective diffusivity D_{eff}. For a sample of geometric area and length L, D_{eff} can be defined by

$$D_{eff} \equiv \frac{N_A \cdot L \cdot RT}{P \cdot (y_{A_1} - y_{A_2})} \qquad (2)$$

Equation (2) was employed in the determination of the effective pellet diffusivity from diffusion measurements in which pure gases are passed over opposite faces of a sample pellet at constant pressure.

In order to relate diffusivity to pore structure, it is convenient to start by considering diffusion in a uniform cylindrical pore.

For Knudsen diffusion, Wheeler (23) gives

$$D = D_{KA} = \frac{2}{3} r \bar{v} \qquad (3)$$

The previous investigations (25) on bulk diffusion were based upon the assumption of equimolal counter diffusion. However, the recent work by Hoogschagen (8), Scott and Dullien (20) and Rothfeld (18) showed that the diffusion fluxes were approximately inversely proportional to the square roots of the molecular weights.

$$\frac{N_A}{N_B} = -\left(\frac{M_B}{M_A}\right)^{\frac{1}{2}} \qquad (4)$$

An expression for bulk diffusion coefficient, based on equation (4), has been derived by Scott and Dullien:

$$D = \frac{D_{AB}}{\alpha (y_{A_1} - y_{A_2})} \ln \frac{1 - \alpha y_{A_2}}{1 - \alpha y_{A_1}} \qquad (5)$$

where $\alpha = 1 - \frac{N_B}{N_A} = 1 - \left(\frac{M_A}{M_B}\right)^{\frac{1}{2}}$

For mixed diffusion, some knowledge of the relative significance of D_{AB} and D_{KA} is required. Correct interpretations have been developed by Rothfeld (18), Scott and Dullien (20) and Wakao and Smith (23). The earlier expressions regarding diffusion in the transition region were:

Wheeler's exponential combining rule (24)

$$D = D_{AB} \left(1 - e^{\frac{-D_{KA}}{D_{AB}}}\right) \qquad (6)$$

and Bosanquet's addition resistance law (15)

$$\frac{1}{D} = \frac{1}{D_{AB}} + \frac{1}{D_{KA}} \tag{7}$$

Equation (7) states that the resistance to transport is the sum of the resistance due to wall and intermolecular collisions. Scott and Dullien (20) claimed that the Bosanquet formula is only valid if two counter diffusion gases have equal molecular weights.

The investigation by Scott and Dullien (20) appears to give an adequate description of diffusion in the transition region. These authors were able to derive an expression for overall diffusivity by considering both the rate of momentum transfer to the wall as well as that arising from unlike collisions. The overall diffusivity related to D_{AB} and D_{KA} is then

$$D = \frac{D_{AB}}{\alpha (y_{A_1} - y_{A_2})} \ln \frac{1 - \alpha y_{A_2} \cdot \frac{D_{AB}}{D_{KA}}}{1 - \alpha y_{A_1} \cdot \frac{D_{AB}}{D_{KA}}} \tag{8}$$

It should be noted that these appropriate expressions for diffusivity are based on a single capillary model. In applying them to porous media, it is customary to consider a certain model of pore structure and introduce the concept of tortuosity X. Effective diffusivities (i.e., diffusivities of porous media) may then be expressed as:

$$D_{eff} = (D_{KA})_{eff} = \frac{2}{3} \bar{r} \bar{v} \varepsilon X \tag{9}$$

$$D_{eff} = (D_{AB})_{eff} = D_{AB} \cdot \varepsilon \, X \qquad (10)$$

It is obvious that $(D_{AB})_{eff}$ is less than the binary gas diffusivity D_{AB} by a factor of ε and X. This is because part of the volume of a porous body referred to is made up of solid rather than free space. On the other hand, X accounts for the increased path length due to the tortuosity of the pore space and other effects which tend to reduce the diffusion rate. The effective diffusivity corresponding to equation (2) can similarly be written as:

$$D_{eff} = \frac{D_{AB} \cdot \varepsilon \, X}{\alpha (y_{A_1} - y_{A_2})} \ln \frac{1 - \alpha y_{A_2} \dfrac{D_{AB}}{D_{KA}}}{1 - \alpha y_{A_1} \dfrac{D_{AB}}{D_{KA}}} \qquad (11)$$

Equation (11) can be employed for the theoretical calculation of D_{eff} over a wide range of pressures from a knowledge of ε, X and average pore radius $\bar{r}$, but applies only to uni-disperse media (i.e., micro or macropores only).

A theory of diffusion in bi-disperse media (i.e. for both micro and macropores) has been recently developed by Wakao and Smith (23) who consider the total rate of transport to be the sum of separate contributions for diffusion through macropores, micropores and a series path. These authors performed diffusion measurements on a series of alumina pellets over the pressure range 1 - 12 atm and obtained good agreement with their theoretical expression. The expression for D_{eff} based on equations (2) and (11) is

$$D_{eff} = \frac{D_{AB}}{\alpha(y_{A_1} - y_{A_2})} \cdot \varepsilon_a^2 \ln \frac{1 - \alpha y_{A_2} + \frac{D_{AB}}{\bar{D}_{K_a}}}{1 - \alpha y_{A_1} + \frac{D_{AB}}{\bar{D}_{K_a}}}$$

$$+ \frac{D_{AB}}{\alpha(y_{A_1} - y_{A_2})} \cdot \varepsilon_i^2 \ln \frac{1 - \alpha y_{A_2} + \frac{D_{AB}}{\bar{D}_{K_i}}}{1 - \alpha y_{A_1} + \frac{D_{AB}}{\bar{D}_{K_i}}}$$

$$+ \frac{D_{AB}}{\alpha(y_{A_1} - y_{A_2})} \cdot \frac{4 \varepsilon_a (1 - \varepsilon_a)}{1 + \frac{(1 - \varepsilon_a)^2}{\varepsilon_i^2}} \cdot$$

$$\ln \frac{1 - \alpha y_{A_2} + \frac{D_{AB}}{\bar{D}_{K_i}} \frac{(1 - \varepsilon_a)^2 / \varepsilon_i^2 + \frac{\bar{D}_{K_i}}{\bar{D}_{K_a}}}{1 + (1 - \varepsilon_a)^2 / \varepsilon_i^2}}{1 - \alpha y_{A_1} + \frac{D_{AB}}{\bar{D}_{K_i}} \frac{(1 - \varepsilon_a)^2 / \varepsilon_i^2 + \bar{D}_{K_i} / \bar{D}_{K_a}}{1 + (1 - \varepsilon_a)^2 / \varepsilon_i^2}} \qquad (12)$$

The first two terms of equation (12) represent the contribution due to macropores and micropores and are similar to that derived by Scott and Dullien (20). If only macro- or micropores exist, equation (12) reduces to the same expression as equation (11). Applicability of this method depends on the proper choice of $\bar{r}$ and X. A detailed

discussion of $\bar{r}$ and X will be given in section C of this chapter.

B. Flow of Gases Through Porous Media

The flow of gases through porous media or so called forced flow is considered to be the flow which results from a total pressure difference across the two ends of the pore channel. This excess pressure will cause a forced flow of molecules which carries the excess number of molecules out of the channel.

Flow has been classified into Knudsen and Poiseuille type. The former is equivalent to the Knudsen diffusion which is not a function of the total pressure. For micropore solids, the pure Knudsen flow occurs even at rather high pressures as shown by the investigations on Vycor glass (2) and Saran Charcoal (6). The Poiseuille flow coefficient depends on total pressure and is a function of the square of the pore radius. In bi-disperse materials, the contribution due to micropores is negligible as compared to the flow through macropores. A plot of K_{eff} vs. P will generally give: (1) a Knudsen flow at pressures approaching zero; (2) a mixed flow at intermediate pressures (0.2 - 5 atm); and (3) a Poiseuille flow at rather high pressures (>5 atm).

The flow of gases through porous materials at laminar flow is governed by Darcy's law which states that the rate of flow is directly proportional to the pressure gradient causing flow. The transport coefficient appearing in Darcy's law is defined as permeability which characterizes the ease with which a fluid may be made to flow by an applied pressure gradient.

For viscous flow, Darcy's law gives

$$Q = -K' \frac{A}{\eta} \frac{dP}{dz} \tag{13}$$

and if the pressure gradient is kept sufficiently small, the effective permeability K'_{eff} in cm^2 can be defined by

$$K'_{eff} \equiv \frac{Q \cdot L \cdot \eta}{\Delta P \cdot A} \tag{14}$$

In order to employ the units of the diffusion coefficient (cm^2/sec) for permeability K, Darcy's law can be written as

$$N_A = - \frac{K}{RT} \cdot \frac{dP}{dz} \tag{15}$$

Since $$N_A = Q \cdot \rho = Q \cdot \frac{P}{RT}$$

then $$K_{eff} \equiv \frac{Q \cdot L \cdot P}{\Delta P \cdot A} \tag{16}$$

where Q is the volumetric flow rate (cm^3/sec) at pressure P(atm), and ΔP is the pressure drop across a sample of length L(cm) and crossectional area $A(cm^2)$.

It can be seen that

$$K_{eff} = \frac{P}{\eta} K'_{eff} \tag{17}$$

Equation (16) permits the determination of effective pellet permeability K_{eff} from forced flow measurements.

It is obvious that permeability defined by Darcy's law is only a macroscopic property of materials. In order to relate permeability to pore structure, the first step is to consider flow through a single

cylindrical pore. A generalized formula which combines the Knudsen and Poiseuille flow has been given by Wheeler (24):

$$N_A = \frac{8\,\Delta P}{3\sqrt{2\pi M RT}\cdot L}\left(r + \frac{3\pi}{64}\,\frac{r}{\lambda}\right) \quad (\text{mole/cm}^2\text{-sec}) \qquad (18)$$

From Darcy's law,

$$N_A = \frac{K\cdot \Delta P}{RT\cdot L} \qquad (15)$$

and $$\eta = \frac{1}{2}\,\rho\,\bar{v}\lambda \;,\; \rho = \frac{PM}{RT}$$

The permeability $K(\text{cm}^2/\text{sec})$ for all ranges may be obtained by combining equations (18) and (15). Thus,

$$K = \frac{2}{3}\,r\,\bar{v} + \frac{r^2 P}{8\eta}\,\varphi \qquad (19)$$

where $$\bar{v} = \sqrt{\frac{8RT}{\pi M}}$$

P = atm

η = dyne-sec/cm^2

φ = conversion factor = 1.013×10^6 $\frac{\text{dynes-sec}}{\text{atm-cm}^2}$

It is seen from equation (19) that

$$K_K = \frac{2}{3}\,r\,\bar{v} \qquad (20)$$

$$K_P = \frac{r^2 P}{8\eta}\,\varphi \qquad (21)$$

when $P = 0$, equation (20) reduces to

$$K = K_K = D_{KA} = \frac{2}{3} r \bar{v} \tag{22}$$

For porous media, the factor of εX is again introduced as in the treatment of diffusion. Equation (19) may thus be written as

$$K_{eff} = \frac{2}{3} \bar{r} \bar{v} \cdot \varepsilon X + \frac{\bar{r}^2 \cdot P}{8 \eta} \varphi \cdot \varepsilon X \tag{23}$$

Equation (23) permits the calculation of effective permeability K_{eff} from the pore structure provided that X can be evaluated. The estimation of $\bar{r}$ and X will be discussed in section C of this chapter.

C. Internal Pore Structure

Porous media in general contain a network of interconnected fine pores which provide a large surface area for chemical reactions. The size of pores has been classified into micropore (< 100 Å) and macropore (> 100 Å). Materials pelleted from powder particles usually contain a large number of micropores which are the void space within the particles themselves. On the other hand, macropores consist of space between particles. The pore size distribution data obtained from mercury penetration (16) provide a useful classification of the type of a medium. Porous media which show only one peak in the pore size distribution plot $\frac{d\varepsilon}{dr}$ vs. r are called uni-disperse systems (i.e., for micro or macropores only). Others which show two peaks, one for macropore and the other for micropore regions are classified as bi-disperse media.

In order to use equation (12) and (23) for interpreting diffusivity and permeability of porous materials, a knowledge of X and average pore radius $\bar{r}$ is required.

The value of X can be obtained from diffusion measurements by applying equation (10) (for uni-disperse media only), and from resistivity measurements (9). However, it is desirable to relate X to pore structure by considering a certain pore model. The characteristics of materials which tend to reduce the flow rate and contribute to X may be due to (1) The tortuosity of path due to the interaction and random distribution of pores.

(2) Pores of varying crossections.

(3) Blind pores.

The early theory relating permeability to pore structure was developed by Kozeny and Carman (5). The well-known Kozeny-Carman equation for the permeability is given as

$$K' = \frac{\varepsilon \cdot r_h^2}{k_o} \left(\frac{L'}{L}\right)^2 \tag{24}$$

where L' = average path length of the flow

L = length of a porous sample

k_o = shape factor

The tortuosity X for this case may be written as

$$X = \frac{1}{k_o} \left(\frac{L'}{L}\right)^2 \tag{25}$$

The values of k_o in various sectional shapes are given in the literature (5). $\left(\frac{L'}{L}\right)$ is an empirical factor which can be determined by electric resistivity measurements. It is seen that Kozeny-Carman

theory accounts for the tortuosity of the pore space as well as the cross-section of pores.

In equation (24), the radius is set equal to the hydraulic radius r_h

$$r_h = \frac{\text{volume filled with fluid}}{\text{wetted surface}} \tag{26}$$

Marshall (11) and Millington and Quirk (13) relate the tortuosity X to structural parameters by considering an interaction model in which the pore channels are imagined to be fully intersected with varying degrees of overlap of the pore crossectional areas. The resulting expression derived by Marshall is

$$K' = \frac{\varepsilon^2}{8n^2}\left\{r_1^2 + 3r_2^2 + 5r_3^2 + \ldots + (2n-1)r_n^2\right\} \tag{27}$$

The relation between X and ε from equation (27) is given by

$$X = \varepsilon \tag{28}$$

The expression given by Millington and Quirk is

$$K' = \frac{\varepsilon^{\frac{4}{3}}}{8n^2}\left\{r_1^2 + 3r_2^2 + 5r_3^2 + \ldots + (2n-1)r_n^2\right\} \tag{29}$$

The tortuosity X for this case may be set as

$$X = \varepsilon^{2/3} \tag{30}$$

In both the theory of Marshall and Millington et al. the average pore radius is given as

$$\bar{r}^2 = \frac{1}{n^2}\left(r_1^2 + 3r_2^2 + 5r_3^2 + \ldots\ldots + (2n-1)\,n^2\right) \quad (31)$$

The value of n represents the classes of radii chosen from pore size distribution data. The larger the value taken for n, the more accurate will be the calculation of $\bar{r}$.

Similar considerations have been applied to pellet diffusion. The recent work by Wakao and Smith (23) arrived at the same result as that of Marshall (11) in which X is equal to ε for media of uni-disperse pore systems. The equation used by Wakao et al. for calculating $\bar{r}$ is

$$\bar{r} = \frac{\int r d\varepsilon}{\varepsilon} \quad (32)$$

The value of $\bar{r}$ determined by equation (32) is the mean integral radius obtained from a knowledge of pore size distribution data.

It should be noted that the work by Marshall, Millington et al. and Wakao et al. is mainly based on the model of periodic constrictions without taking the tortuous path into consideration. None of these theories consider blind pores.

Other expressions relating X to ε, based on the tortuous path of diffusion only, have been proposed by various workers. Some of these theories have been reviewed and tested by Masamune and Smith (12) who performed diffusion measurements in a series of silver pellets and correlated their data with the following expression:

$$X = \frac{C}{C + (1 - \varepsilon_a)} \quad (33)$$

where C is a constant and ε_a is the macropore volume.

The investigation by Buckingham (4) also gives the same result as that by Marshall

$$X = \varepsilon \tag{28}$$

Wheeler (24) has calculated the tortuous path value X by assuming random pore directions. If pores are completely in random orientation, the average direction of the flow path may be at an angle of 45° with its crossection as axis. Thus,

$$X = \frac{1}{\sqrt{2}} \tag{34}$$

Other methods for estimating the average pore radius $\bar{r}$ have been proposed by various authors. One of those methods based upon straight cylindrical pores of constant length has been given (21) as

$$\bar{r} = \frac{2\varepsilon}{S} \tag{35}$$

When a normal distribution curve with a sharp peak exists, $\bar{r}$ may be considered as a most probable radius which can be obtained from pore size distribution plots ($\frac{d\varepsilon}{dr}$ vs. r). This method of estimating $\bar{r}$ has been used by Rothfeld (18) and Amberg, et al. (1).

Equations (26) and (35) provide a proper estimation of $\bar{r}$ when the materials have a small range of pore sizes such as microporous solids and unconsolidated media. All these methods will not give good results if the materials have a wide range and a random distribution of pore sizes. For such materials, the method used by Wakao et al. may give a better estimation of $\bar{r}$ than other methods.

IV - EXPERIMENTAL ASPECTS OF DIFFUSIVITY AND PERMEABILITY

A. Experimental Apparatus and Procedure

The high pressure diffusion apparatus shown schematically in Figure 1 is similar in principle to that of Wicke and Kallenbach (25) who measured counter diffusion rates through porous materials by passing pure gases over opposite faces of a sample pellet. The pressure at both faces of the pellet was maintained at the same value. The diffusion cell D and the differential manometer M_1 were designed for holding pressures of up to 100 atm. High pressure fittings and 1/8" stainless steel tubings (Autoclave Engineering Sales Corp., Erie, Pennsylvania) were used for all connections.

A plexi-glass disk with a sample pellet was set in the diffusion cell D for measurements. For detailed description of the cell D and the assembly of pellets, refer to Figure 2. The pressure at both faces of the sample was maintained at the same value either by controlling the inlet flow rates with needle valves v_1, v_2 and v_3, v_4 (2MA, Nupro Metering Valve, Nuclear Products Co., Cleveland, Ohio) or by controlling the outlet flow rate with needle valve v_6. A plexi-glass U-tube manometer M_1 connected to both sides of the cell D served as pressure sensing device. This manometer which held pressures of up to 100 atm was made by drilling two channels of 1/8" diameter through a plexi-glass block (5" x 6" x 2"). Each end of the channel was connected to an adapter (TA-2201, Autoclave Engineering Sales Corp., Erie, Pennsylvania). In order to eliminate the pressure heads caused by the density difference between hydrogen and nitrogen gases, precautions were taken to locate M_1 and D with a minimum of head difference, and to reduce the unnecessary dead space between them.

The hydrogen gas diffusing through the sample pellet into the nitrogen stream was analyzed quantitatively by the thermal conductivity cell C as shown in Figure 1. The nitrogen stream then flowed past the capillary flow meter F_1 and the flow manometer M_2. A soap film meter was employed to measure flow rates of the nitrogen stream at atmospheric pressure. The hydrogen stream flowed past the capillary flow meter F_2 and the flow manometer M_3. The cell C served for analyzing the nitrogen stream only. No analysis of the hydrogen stream was made. The value of α was determined by applying equation 4.

Needle valves v_{15} - v_{17} (2 RB 280, Metering Valve, Hoke Inc., New Jersey) and U-tube manometer M_4 - M_5 containing mercury were the auxiliary equipment for diffusivity measurements at pressures below atmospheric. The needle valve v_{15} connected to a vacuum pump was used to control the subatmospheric pressure indicated by M_4. Flow rates of the nitrogen stream based on the particular subatmospheric pressure indicated by M_5 were calibrated with a soap film meter.

Some difficulty was experienced in accurately measuring diffusivities at elevated pressures (>30 atm) due to the increased sensitivity of the pellets to forced flow permeation. The pressure on each side of the pellet was then maintained at exactly the same value ($\pm$ 0.5 mm oil) by carefully manipulating the control needle values v_1 - v_6.

For permeability measurements, the steady state method as described by Lea and Nurse (10) was used. Permeabilities were measured by establishing linear flow through the sample pellet and applying Darcy's law as given by equation (16). The diffusion apparatus was used for measuring permeability with the following modifications:

valves v_4 and v_5 and the thermal conductivity cell C were kept closed. Pure nitrogen was supplied continuously to the cell D. The valve v_8 was first closed and the gas was allowed to flow out of the cell C until a desired pressure drop had been developed. The value of pressure difference was observed from the oil (Specific Gravity = 1.75) or mercury-filled glass U-tube manometer M_1 (10AA25WM, Meriam Instrument Co., Cleveland, Ohio). For high pressure runs (>30 atm) M_1 was replaced by a plexi-glass manometer. The flow which resulted from the pressure difference then emerged through the valve v_6 and the capillary flow meter F_2. It was essential to reduce the flow rate or enlarge the pellet area whenever the pressure drop required for forcing the flow through the pellet was too large.

Diffusivities and permeabilities of porous materials were determined from the measured values by applying equations (2) and (16) respectively. The mole fraction of hydrogen y_{A_2} and the flow rate of the nitrogen stream Q were obtained from the analysis of the cell C and the flow meter M_2. The length L and the area A were determined by a micrometer. The values of ΔP were observed from M_1. Sample calculations will be given in the Appendix.

B. The Diffusion Cell and the Mounting of Sample Pellets

The diffusion cell was made of brass and consisted of two threaded cylindrical chambers which screwed into each other. Provision was made in one of the chambers to place 1/8" plexi-glass disk with tested pellets. While in operation, these chambers were sealed off from each other and from the surroundings by compressing each side of the plexi-glass disk with a rubber O-ring as shown in Figure 2.

The sample porous pellets were sealed into a plexi-glass disk by means of epoxy resin (The Shell Chemical Co., Montreal, Que.). This method of mounting had the advantage that it was good for pressures up to 100 atm, and that it could be used for pellets of other than cylindrical shape. Pellets of the same kind were mounted on several disks for testing the reproducibility of the pellets themselves and the technique of mounting. In order to obtain average values from the commercial pellets, sets of 3 pellets were mounted on each disk except for Columbia Carbon SXC 2/4, Molecular Sieve 4A 35000 psi, and Vycor glass because these materials have fairly uniform pore properties. All except SXC 4/6 and Molybdena Alumina Catalyst were mounted in both axial and radial directions with either their faces or their circumference exposed.

C. The Thermal Conductivity Cell and the Analysis of Gas Mixture

The conductivity cells were made of two parallel 3/16" channels drilled through an insulated aluminum cylinder, $3\frac{1}{2}$" x 2". Each end of these channels were connected to a 1/8" copper tubing. One of the channels containing pure nitrogen was the reference cell. The other channel served for analyzing the gas mixture. In order to reduce the effect of flow rate, this channel was located as a by-pass of the nitrogen stream ($H_2 + N_2$) as shown in Figure 1. The cells were heated slightly above room temperature by a heating wire which was controlled by two powerstat transformers. The temperature of the cells was maintained constant by a "Thermistemp" temperature controller (63 RB. Yellow Springs Instrument Co. Inc., Yellow Springs, Ohio) in which the temperature was sensed by means of a thermistor probe (76A, Keystone Carbon, St. Mary's, Pennsylvania). A thermistor (A-33, Victory Engineering Corp., New Jersey) was sealed into each of these channels to form a Wheatstone bridge with two standard

resistances. The unbalance of the Wheatstone bridge due to a difference in thermal conductivity between the reference cell (N_2) and the nitrogen stream ($H_2 + N_2$) was recorded by a potentiometer (3184-D, Tinsley Instruments, Smith Falls, Ontario).

Values of the mole fraction of H_2 in the nitrogen stream were obtained from the potentiometer readings. To calibrate the potentiometer reading of e.m.f. against the composition of the nitrogen stream, a prepared mixture ($H_2 + N_2$) of known composition was passed continuously through the conductivity cell until a steady reading of e.m.f. had been obtained.

D. Pore Structure Data

Pore size distribution data were obtained from mercury penetration down to a radius of 20 Å (26). The plots of ε vs. r and $\frac{\Delta \varepsilon}{\Delta \log r}$ vs. r are shown in Figure 3 - Figure 7. Numerical values are given in Table 5.

Macropore volumes were obtained from mercury penetration data as cumulative pore volumes. For materials having sizes smaller than 20 Å, micropore volumes were determined by the helium penetration method, and average micropore radii determined from B.E.T. surface area.

Pellet densities were determined from geometric volumes and weights of pellets.

E. Materials Used

Seven types of porous material were used in this investigation. All except Molecular Sieve 4A and Vycor glass are commercial pellets. Properties of these materials are summarized in Table 6.

1. Columbia Activated Carbon
   SXC 2/4, Union Carbide Canada Limited, Toronto.

2. Columbia Activated Carbon
   SXC 4/6, Union Carbide Limited, Toronto.

3. Copper Chromite Catalyst
   Cu 0203 T 3/16", Harshaw Chemical Co., Cleveland, Ohio.

4. Molybdena Alumina Catalyst
   Mo - 1201 T 3/16", Harshaw Chemical Co., Cleveland, Ohio.

5. Nickel Catalyst
   Kieselguhr Ni 0704 E 5/32", Harshaw Chemical Co., Cleveland, Ohio.

6. Molecular Sieve 4A 35000 psi
   Pelleted at 35000 psi from Molecular Sieve 4A powder, Linde Co., Division of Union Carbide Corporation.

7. Vycor Glass
   No. 7930, Brand, Corning Glass Works, Corning, New York.

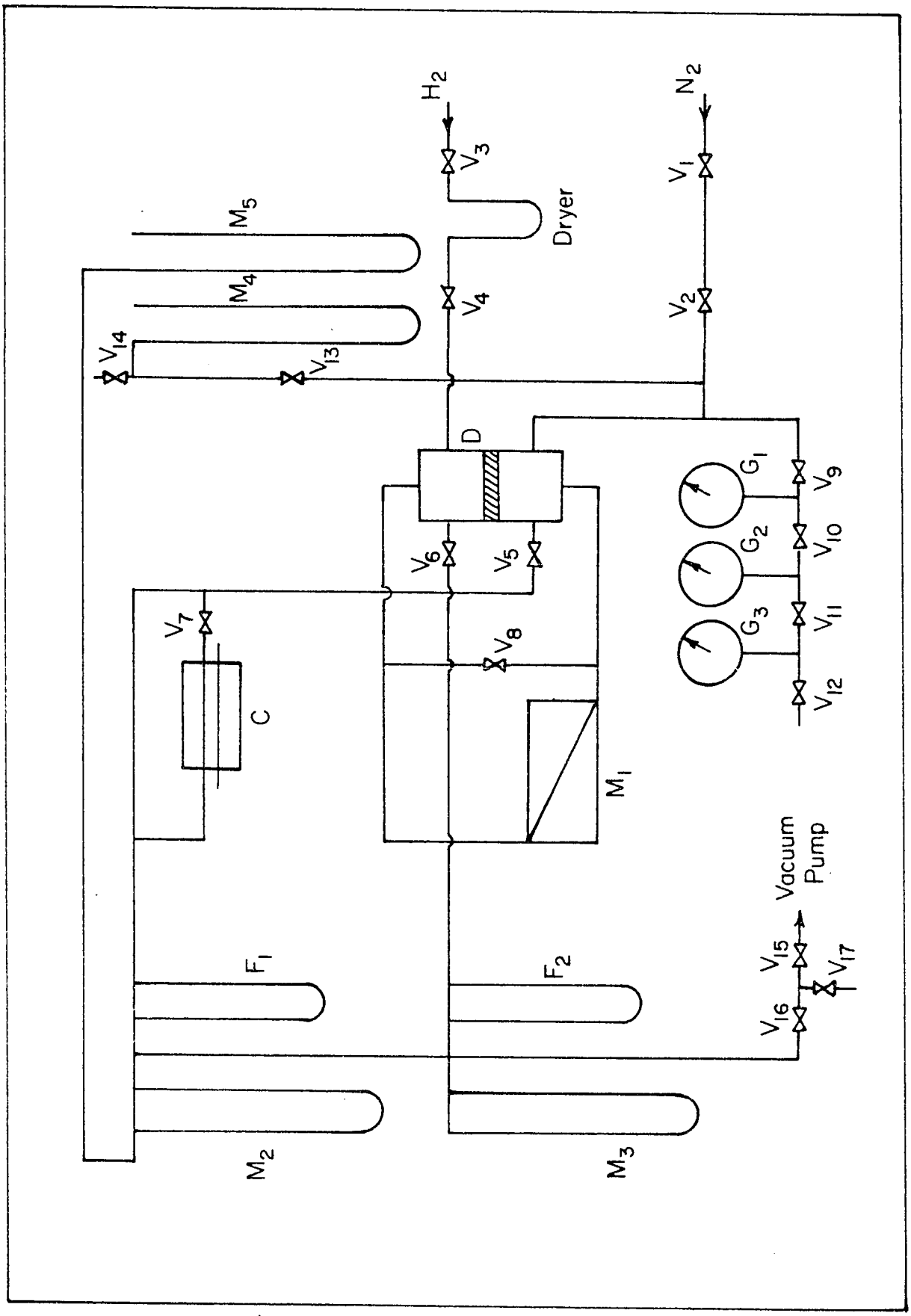

Fig. 1. Apparatus for Measuring Diffusivity and Permeability in Porous Solids at Varying Total Pressures

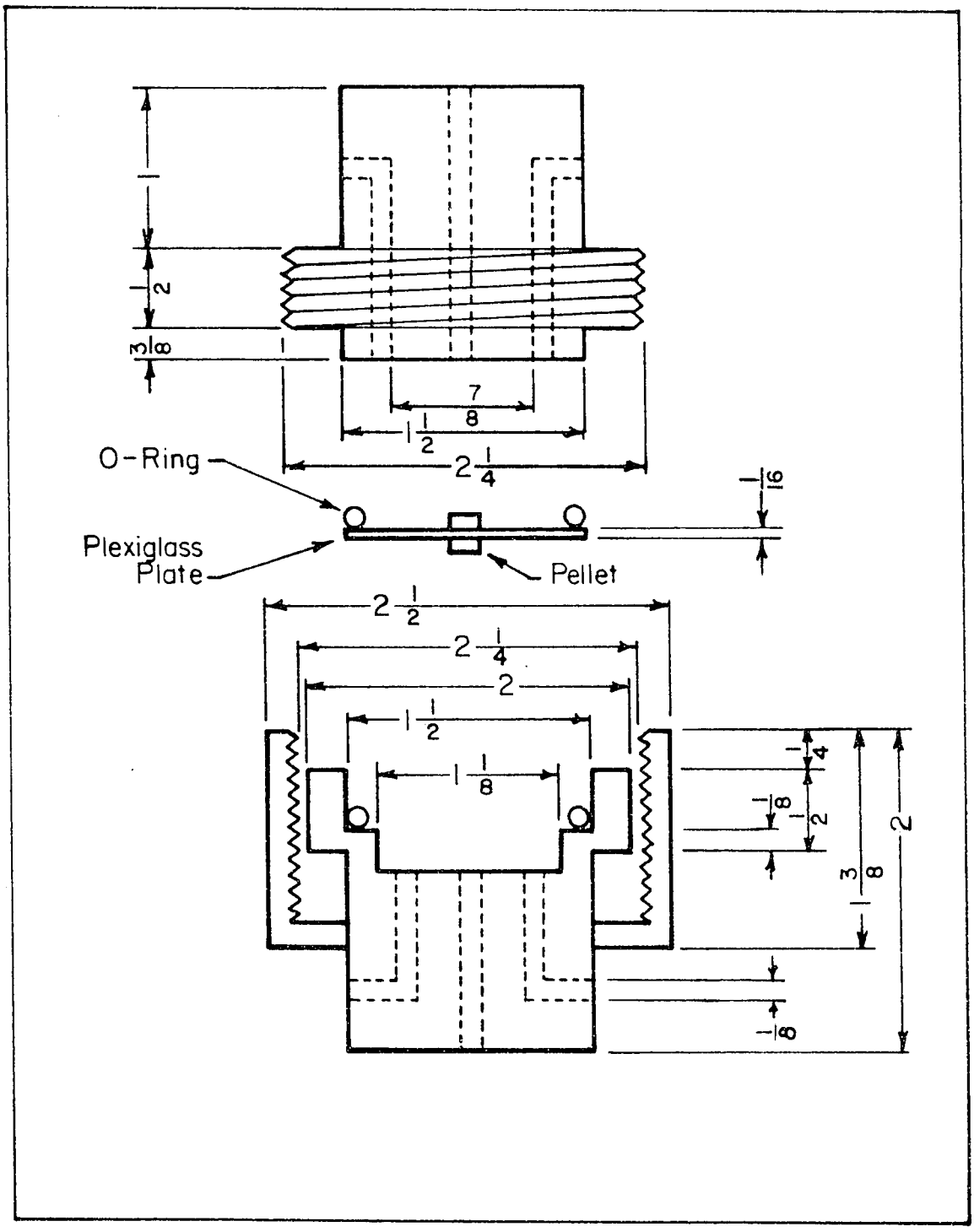

Fig. 2. High Pressure Diffusion Cell

V - RESULTS

Table 1. Diffusivity Data, Axial

$H_2 - N_2$

T = 25°C

(a) Molecular Sieve 4A, 35000 psi

Pellet No.	P (atm)	Q (cm^3/sec)	y	D_{eff} (cm^2/sec)
M.S. 4A-1	0.136	1.20	0.054	0.612
L = 0.378 cm	0.214	1.23	0.070	0.5265
A = 0.311 cm	0.369	2.20	0.055	0.4215
	0.664	4.13	0.040	0.3170
	1.495	4.0	0.0505	0.173
	1.950	2.76	0.0724	0.1341
	3.40	3.90	0.0577	0.0853
	6.23	4.42	0.0565	0.0517
	7.40	3.35	0.0690	0.0408
	15.98	3.84	0.0625	0.0195
	35.0	4.52	0.048	0.00793
	57.1	3.70	0.051	0.00423
	98.7	2.63	0.0646	0.00223
(b) Columbia Carbon SXC 2/4				
C (2/4) - 1	0.125	0.515	0.059	0.1723
L = 0.361	0.135	0.540	0.056	0.1583
A = 0.541	0.184	0.357	0.1015	0.146
	0.326	1.090	0.041	0.0955
	0.350	1.0	0.042	0.0838
	0.582	1.70	0.029	0.05813
	0.652	1.15	0.0414	0.0509

cont....

Table 1 (continued)

Pellet No.	P (atm.)	Q (cm^3/sec)	y	D_{eff} (cm^2/sec)
C (2/4) - 1	1.095	2.02	0.027	0.0342
L = 0.361	3.230	1.092	0.0535	0.01275
A = 0.541	6.11	1.16	0.051	0.00681
	55.0	1.17	0.0362	0.000533
C (2/4) - 2	2.29	2.11	0.029	0.0195
L = 0.384	4.81	2.12	0.0257	0.00825
A = 0.541	22.2	1.072	0.048	0.00173
(c) Nickel Catalyst				
Ni - 1	0.123	1.23	0.075	0.463
L = 0.2076	0.169	1.22	0.0862	0.388
A = 0.363	0.224	1.99	0.0630	0.3406
	0.429	2.44	0.0673	0.2344
	1.208	2.35	0.092	0.1128
	3.40	5.07	0.0565	0.0511
	6.12	4.4	0.070	0.0309
Ni - 2	34	4.30	0.0495	0.004767
L = 0.263	56	4.30	0.0442	0.002573
A = 0.363	83	4.20	0.0405	0.00155
	102.6	4.21	0.0415	0.001284
Ni - 3	0.48	4.55	0.019	0.2143
L = 0.423	0.718	4.46	0.0223	0.165
A = 0.363				

cont....

Table 1 (contimued)

(d) Copper Chromite Catalyst

Pellet No.	P (atm)	Q (cm^3/sec)	y	D_{eff} (cm^2/sec)
Cu - 1	0.2963	4.0	0.032	0.294
L = 0.358	0.517	3.96	0.0427	0.226
A = 0.542	0.764	5.10	0.04	0.184
	2.91	8.81	0.0382	0.079
	11.43	4.64	0.0898	0.0264
	20	5.04	0.0876	0.01593
Cu - 2	0.202	2.80	0.053	0.486
L = 0.34	0.309	4.47	0.045	0.429
A = 0.542	0.417	4.47	0.051	0.362
	0.70	4.93	0.051	0.237
	1.83	8.54	0.039	0.119
	2.22	6.37	0.0564	0.1075
	6.30	8.03	0.050	0.0421
	11.80	6.46	0.068	0.02518
	20.40	6.45	0.068	0.0145
Cu - 3	6.3	6.5	0.0622	0.0473
L = 0.376				
A = 0.542				

cont. . . .

Table 1 (continued)

(e) Columbia Carbon SXC 4/6

Pellet No.	P (atm)	Q (cm^3/sec)	y	D_{eff} (cm^2/sec)
C (4/6) - 1	0.257	0.275	0.077	0.134
L = 0.406	0.465	0.276	0.0896	0.0875
A = 0.27	0.603	0.81	0.0353	0.0738
	0.80	1.12	0.026	0.0562
	2.29	0.61	0.051	0.0215
	4.74	0.61	0.0515	0.0106
	6.05	0.49	0.068	0.0088
	12.10	0.96	0.0352	0.00434
	20.30	0.79	0.0412	0.00252
C (4/6) - 2	0.1715	0.50	0.0434	0.1625
L = 0.34	0.3287	0.752	0.044	0.1292
A = 0.277	0.536	0.67	0.054	0.0875
	0.81	1.01	0.0362	0.0576
	2.2	1.05	0.041	0.02507

(f) Vycor glass

Vycor - 1	0.279	0.108	0.018	0.00262
L = 0.467	0.72	0.167	0.0305	0.00268
A = 1.266	0.906	0.193	0.0317	0.00257
	2.243	0.54	0.027	0.00246
	6.21	1.95	0.0188	0.00217
	12.2	1.092	0.053	0.00185
	23.1	2.165	0.041	0.001482
	34.3	2.35	0.049	0.00130
	47.2	3.10	0.044	0.00115
	65.6	3.53	0.043	0.00089

Table 1 (continued)

(g) Molybdena Alumina Catalyst

Pellet No.	P (atm)	Q (cm^3/sec)	y	D_{eff} (cm^2/sec)
Mo - 1	0.1745	0.398	0.0245	0.0437
L = 0.38	0.258	0.404	0.031	0.0383
A = 0.498	0.408	0.644	0.0267	0.033
	0.485	0.67	0.0317	0.0346
	0.715	1.135	0.0222	0.0276
	0.80	1.15	0.0244	0.0274
	1.877	2.13	0.0250	0.0222
	2.29	2.15	0.027	0.0199
	4.1	2.30	0.0346	0.01534
	6.03	2.33	0.0413	0.0127
	10.3	2.615	0.049	0.00998
	20.4	2.95	0.0577	0.006765
	31.9	4.0	0.0514	0.00518
	50.6	4.43	0.055	0.00389
Mo - 2	2.09	2.185	0.0292	0.0230
L = 0.364	4.74	2.16	0.041	0.0143
A = 0.498				
Mo - 3	0.165	0.435	0.0266	0.0536
L = 0.37	0.353	0.64	0.0325	0.0451
A = 0.498	0.522	0.663	0.042	0.0395
	0.779	0.97	0.0345	0.0331
	2.29	2.2	0.031	0.0228
	5	2.23	0.0453	0.01565
	10.66	2.90	0.0475	0.01005

cont....

Table 1 (continued)

Pellet No.	P (atm)	Q (cm^3/sec)	y	D_{eff} (cm^2/sec)
Mo - 3	22.8	3.10	0.062	0.006685
L = 0.37	32	4.2	0.0527	0.00542
A = 0.498				
Mo - 4	0.14	0.133	0.0695	0.0421
L = 0.305	0.321	0.33	0.0634	0.0416
A = 0.51	0.597	0.525	0.0537	0.02986
	2.09	1.19	0.055	0.01972
	3.24	2.54	0.0334	0.0163

Table 2. Diffusivity Data, Radial

$H_2 - N_2$

T = 25°C

(a) Molecular Sieve 4A, 35000 psi

Pellet No.	P (atm)	Q (cm^3/sec)	y	D_{eff} (cm^2/sec)
M.S. 4A - 1 R				
L = 0.418	0.216	0.802	0.066	0.4985
A = 0.22	0.669	1.48	0.062	0.278
	2.22	2.80	0.0526	0.133
	14.75	2.96	0.049	0.0196
	32.50	3.05	0.0464	0.00867
(b) Columbia Carbon SXC 2/4				
C (2/4) - 1 R	0.276	0.45	0.04	0.115
L = 0.50	0.922	0.315	0.0705	0.0425
A = 0.305	2.28	1.175	0.0244	0.0211
C (2/4) - 2 R	0.713	0.38	0.0812	0.0663
L = 0.5	2.29	0.76	0.049	0.02408
A = 0.355	6.11	0.84	0.047	0.00955
C (2/4) - 3 R	2.22	1.85	0.0166	0.0227
L = 0.45	4.74	2.19	0.015	0.01135
A = 0.279				

Table 2 (continued)

(c) Nickel Catalyst

Pellet No.	P (atm)	Q (cm^3/sec)	y	D_{eff} (cm^2/sec)
Ni - 1R				
L = 0.297				
A = 0.39	0.3460	1.488	0.0750	0.266
	0.536	1.99	0.0733	0.223
	0.732	2.13	0.0775	0.186
	2.20	4.27	0.0562	0.088
	6.24	4.25	0.0658	0.0365
(d) Copper Chromite Catalyst				
Cu - 2R	0.731	7	0.04	0.277
L = 0.30	0.449	4.65	0.0461	0.347
A = 0.432	2.0	8.2	0.0418	0.1242
Cu - 3R	0.166	2.65	0.064	0.663
L = 0.265	0.3494	6.25	0.037	0.418
A = 0.4357	0.498	5.95	0.044	0.337
	0.802	8.15	0.040	0.257
	2.12	9.15	0.0407	0.112
	4.27	6.50	0.068	0.0675
	7.90	7.265	0.068	0.0407
	13.17	7.0	0.071	0.0247
	21.40	6.35	0.080	0.00157

Table 2 (continued)

(e) Vycor glass

Pellet No.	P (atm)	Q (cm^3/sec)	y	D_{eff} (cm^2/sec
Vycor - 1 R	2.305	0.372	0.0128	0.00196
L = 0.52	3.96	0.384	0.02	0.00188
A = 0.555	5.08	0.385	0.025	0.00182
	6.98	0.415	0.0294	0.00169
	10.30	0.428	0.0376	0.00153
	20	0.45	0.058	0.001295
	36.3	0.892	0.043	0.001034
	63.2	0.932	0.052	0.000758

Table 3. Permeability Data, Axial

N_2

T = 25°C

(a) Molecular Sieve 4A, 35000 psi

Pellet No.	P (atm)	Q (cm^3/sec)	ΔP (atm)	K_{eff} (cm^2/sec)
M.S. 4A-1	0.202	0.062	0.183	0.412
L = 0.378	0.296	0.06	0.155	0.47
A = 0.311	0.596	0.14	0.282	0.605
	0.727	0.208	0.380	0.665
	0.913	0.10	0.174	0.070
	1.25	0.109	0.150	0.883
	1.55	0.247	0.288	1.04
	1.61	0.113	0.129	1.06
	2.51	0.129	0.1056	1.49
	2.80	0.345	0.264	1.59
	3.44	0.330	0.211	1.90
	4.76	0.40	0.195	2.50
	7.56	0.55	0.164	4.07
	7.56	0.863	0.2574	4.08
	15.40	0.93	0.150	7.53
	28.20	3.25	0.272	14.50
	39.10	3.90	0.230	20.60
	40.40	3.60	0.204	21.50
	47.40	4.94	0.2366	25.40
	53.30	3.80	0.1615	28.60
	62.80	3.15	0.1087	35.30
	68.70	3.72	0.1156	39.10
	74.50	5.77	0.163	43.10
	74.70	4.35	0.1216	43.50

cont....

Table 3 (continued)

Pellet No.	P (atm)	Q (cm^3/sec)	ΔP (atm)	K_{eff} (cm^2/sec)
M.S. 4A - 1	80.60	0.70	0.0163	52.2
L = 0.378	89.85	0.73	0.01456	60.9
A = 0.311	101.20	0.87	0.0150	70.5
(b) Columbia Carbon SXC 2/4				
C (2/4) - 1				
L = 0.361				
A = 0.541	0.401	0.19	0.163	0.78
	0.649	0.315	0.177	1.19
	2.97	1.05	0.1775	3.95
	7.22	0.57	0.0363	10.50
	7.22	0.843	0.0542	10.40
	22.1	2.55	0.0563	30.30
	33.3	2.8	0.0411	45.5
	47.3	3.63	0.0385	63.0
	59.9	3.35	0.0285	78.5
	69.7	3.20	0.0236	90.50
C (2/4) - 2	0.22	0.055	0.0836	0.466
L = 0.384	0.40	0.103	0.114	0.642
A = 0.541	0.571	0.087	0.0668	0.925
	0.68	0.1235	0.0856	1.025
	0.732	0.145	0.0883	1.167
	0.82	0.145	0.0877	1.175
	1.176	0.37	0.1645	1.595

cont. . . .

Table 3 (continued)

Pellet No.	P (atm)	Q (cm^3/sec)	ΔP (atm)	K_{eff} (cm^2/sec)
C (2/4) - 2	1.50	0.418	0.145	2.04
L = 0.384	1.63	0.34	0.111	2.18
A = 0.541	2.157	0.58	0.147	2.80
	3.15	0.46	0.0856	3.81
	3.66	0.55	0.087	4.50
	5.98	1.0	0.0902	7.88
	7.8	1.04	0.0735	10.0
	14	3.22	0.1366	16.77
	21.70	3.05	0.07665	28.3
	33.6	6.55	0.0963	48.3
(c) Nickel Catalyst				
Ni - 3	0.44	0.0442	0.198	0.261
L = .423	0.542	0.0473	0.198	0.2785
A = 0.363	0.734	0.0468	0.1715	0.318
	0.921	0.0517	0.168	0.359
	1.12	0.0496	0.148	0.394
	1.66	0.0575	0.135	0.495
	2.10	0.1025	0.206	0.578
	3.40	0.1175	0.171	0.80
	4.57	0.108	0.125	1.006
	7.80	0.1375	0.101	1.59
	9.52	0.39	0.24	1.89
	13.50	0.42	0.188	2.62
	16.50	0.45	0.163	3.22
	21.40	0.535	0.1485	4.20

Table 3 (continued)

Pellet No.	P (atm)	Q (cm^3/ sec)	ΔP (atm)	K_{eff} (cm^2/ sec)
Ni - 4	7.07	0.375	0.261	1.44
L = .363	20.70	0.940	0.241	3.90
A = 0.363	42.50	0.392	0.0537	7.30
	47.50	0.392	0.0483	8.12
Ni - 5	8.2	0.46	0.318	1.36
L = .34	14.50	0.80	0.319	2.35
A = .363	27.50	1.84	0.40	4.31
	48.90	2.35	0.301	7.32
	61.1	2.70	0.281	9.0
	75.0	2.75	0.237	10.8
	87.1	0.265	0.01844	13.45
	96.2	0.255	0.01584	15.0
Ni - 6	2.02	0.085	0.176	0.573
L = 0.43	4.25	0.134	0.156	0.1015
A = 0.363	6.44	0.40	0.35	1.354
	11.30	0.542	0.28	2.29
	16.90	0.69	0.24	3.42

cont....

Table 3 (continued)

(d) Copper Chromite Catalyst

Pellet No.	P (atm)	Q (cm^3/sec)	ΔP (atm)	K_{eff} (cm^2/sec)
Cu - 1	0.492	0.04	0.143	0.185
L = 0.358	0.61	0.039	0.130	0.198
A = 0.542	0.80	0.044	0.139	0.209
	1.18	0.08	0.203	0.26
	1.34	0.125	0.2943	0.28
	2.2	0.098	0.174	0.372
	3.08	0.141	0.199	0.47
	6.36	0.408	0.348	0.772
	11.30	0.61	0.315	1.278
	14.60	0.705	0.289	1.61
	19.25	0.712	0.222	2.106
Cu - 2	0.40	0.095	0.212	0.281
L = 0.34	0.62	0.09	0.174	0.317
A = 0.542	0.734	0.098	0.182	0.339
	0.870	0.10	0,1725	0.363
	1.18	0.1032	0,156	0,415
	1.47	0.1167	0.159	0.46
	1.932	0.111	0.1275	0.546
	2.53	0.140	0.138	0.635
	3.84	0.139	0.106	0.822
	6.41	0.52	0.268	1.217
	11.30	0.59	0.1873	1.975
	19.65	0.779	0.1414	3.48

Table 3 (continued)

Pellet No.	P (atm)	Q (cm^3, sec)	ΔP (atm)	K_{eff} (cm^2, sec)
Cu - 3	3.17	0.137	0.20	0.474
L = 0.376	7.87	0.46	0.329	0.970
A = 0.542	12.83	0.54	0.2484	1.51
	18.50	0.686	0.228	2.09
(e) Columbia Carbon SXC 4/6				
C (4/6) - 1	0.33	0.09	0.1875	0.721
L = 0.406	0.463	0.102	0.170	0.906
A = 0.27	0.56	0.110	0.159	1.04
	0.61	0.113	0.155	1.096
	0.708	0.125	0.154	1.22
	1.04	0.145	0.1310	1.67
	1.52	0.137	0.089	2.31
	1.76	0.40	0.235	2.57
	3.16	0.55	0.203	4.07
	5.90	0.56	0.1077	7.82
	11.0	0.98	0.105	14.0
	20.0	1.13	0.0683	24.9
C (4/6) - 2	0.910	0.18	0.1356	1.62
L = 0.34	0.715	0.155	0.1446	1.32
A = 0.277	3.160	0.44	0.1203	4.50
	7.185	0.55	0.071	9.50
	11.30	2.51	0.204	15.1

Table 4. Permeability Data, Radial

N_2

T = 25° C

(a) Molecular Sieve 4A

Pellet No.	P (atm)	Q (cm^3/sec)	ΔP (atm)	K_{eff} (cm^2/sec)
M.S. 4A - 1 R	0.54	0.049	0.148	0.587
L = 0.39	0.827	0.051	0.119	0.76
A = 0.22	1.45	0.0982	0.153	1.137
	3.11	0.255	0.221	2.043
	6.41	0.49	0.230	3.78
	11.42	0.69	0.185	6.61
	19.44	1.01	0.1553	11.52

(b) Columbia Carbon SXC 2/4

C (2/4) - 1 R	5.08	0.54	0.1156	7.66
L = 0.5	10.	2.54	0.287	14.5
A = 0.305	19.44	3.1	0.181	28.1
C (2/4) - 2 R	1.433	0.297	0.123	3.4
L = 0.50	3.13	0.56	0.1096	7.23
A = 0.355	5.10	0.56	0.0655	12.02
	9.52	1.09	0.0716	21.40
	19.44	3.32	0.1067	43.85

CONT....

Table 4 (continued)

(c) Nickel Catalyst

Pellet No.	P (atm)	Q (cm^3/sec)	ΔP (atm)	K_{eff} (cm^2/sec)
Ni - 1 R	0.380	0.048	0.14	0.2608
L = 0.297	0.631	0.05	0.125	0.305
A = 0.39	0.64	0.0475	0.122	0.298
	0.842	0.051	0.117	0.333
	1.37	0.0642	0.1028	0.476
	3.0	0.268	0.2708	0.753
	4.52	0.337	0.247	1.042
	10.50	0.56	0.1872	2.28
	17.66	0.67	0.144	3.54
	21.7	0.74	0.1337	4.22

(d) Copper Chromite Catalyst

Cu - 1 R	3.17	0.456	0.315	1.255
L = 0.3	6.41	0.59	0.2324	2.20
A = 0.3458	11.4	0.73	0.1754	3.61
	14.63	0.80	0.149	4.66
	19.20	0.916	0.130	6.11
Cu - 2 R	0.602	0.097	0.0988	0.681
L = 0.30	0.888	0.135	0.117	0.803
A = 0.432	1.62	0.38	0.234	1.12
	3.18	0.485	0.182	1.854
	5.74	0.475	0.1146	2.874
	7.90	0.630	0.1185	3.712

cont....

Table 4 (continued)

Pellet No.	P (atm)	Q (cm^3/sec)	ΔP (atm)	K_{eff} (cm^2/sec)
Cu - 2R				
L = 0.30				
A = 0.432				
	11.30	0.825	0.113	5.06
	14.62	0.930	0.101	6.385
	18.0	1.03	0.0943	7.582
Cu - 3R	0.29	0.08	0.121	0.402
L = 0.265	0.45	0.10	0.13	0.468
A = 0.4357	0.65	0.116	0.131	0.539
	0.86	0.106	0.1063	0.606
	1.04	0.106	0.0977	0.660
	1.24	0.1052	0.0890	0.720
	1.49	0.202	0.146	0.840
	2.10	0.135	0.0810	1.013
	5.715	0.442	0.119	2.26
	10.34	0.722	0.112	3.92
	20.	1.33	0.1083	7.47

Table 5. Pore Volume - Pore Size Distribution Data

(a) Columbia Carbon SXC 4/6

radius r (Å)	Cumulative Pore Volume (cc/cc)
56,000	0
20,830	0.0533
14,700	0.0733
10,752	0.08677
8,475	0.0966
5,952	0.1086
4,587	0.1142
3,145	0.1182
2,392	0.1196
1,930	0.1217
1,618	0.1228
1,392	0.1233
1,000	0.125
330	0.1318
200	0.137
100	0.1465
50	0.169
33	0.1835

(b) Copper Chromite Catalyst

radius r (Å)	Cumulative Pore Volume (cc/cc)
56,000	0
20.830	0
14,700	0.0261
10,752	0.01003
8,475	0.02667
5,952	0.02159
4,587	0.03284
3,145	0.073
2,392	0.1888
1,930	0.30246
1,618	0.3694
1,392	0.3917
1,000	0.4078
330	0.4138
200	0.40
100	0.3858
50	0.40
33	0.429
25	0.4376

Table 5 (continued)

(c) Columbia Carbon SXC 2/4

radius r (Å)	Cumulative Pore Volume (cc/cc)
68,000	0
20,000	0.106
10,000	0.138
3,333	0.159
1,000	0.166
500	0.172
333	0.172
200	0.172
100	0.179
50	0.193
33	0.20
25	0.207
20	0.221

(d) Molecular Sieve 4A

radius r (Å)	Cumulative Pore Volume (cc/cc)
68,000	0
10,000	0.0192
3,330	0.355
1,000	0.405
500	0.412
333	0.412
200	0.412
100	0.412
50	0.422
33	0.422
25	0.422
20	0.422

Table 5 (continued)

(e) Nickel Catalyst

radius r (Å)	Cumulative Pore Volume (cc/cc)
8,500	0
3,200	0.253
1,000	0.425
500	0.4715
300	0.482
250	0.482
200	0.482
100	0.482
50	0.482
33	0.482
25	0.482
20	0.482

(f) Molybdena Alumina Catalyst

radius r (Å)	Cumulative Pore Volume (cc/cc)
3,300	0
1,000	0.144
500	0.1585
330	0.1585
250	0.1585
200	0.1585
100	0.1585
50	0.245
33	0.4465
25	0.461
20	0.461

Table 6. Properties of Porous Materials

Materials	Pellet density g/cm³	Total Void Fraction	Pore Volume (cc/cc)		Average pore radius (Å)					
			Micropore ε_i	Macropore ε_a	Micropore $\bar{r}_i$	Macropore $\bar{r}_a$				X
						$(\bar{r}_a)_1$	$(\bar{r}_a)_2$	$(\bar{r}_a)_3$	$(\bar{r}_a)_4$	
Carbon SXC 2/4	0.69	0.795	0.623	0.172	20	27000	33200	30000	24800	0.164
Carbon SXC 4/6	0.69	0.752	0.583	0.169	20	23000	27300	32000	25400	0.1742
Copper Chromite Catalyst	3.4	0.429	0	0.429	0	3200	5600	2400	3480	0.437
Molybdena Alumina Catalyst	1.44	0.461	0.3025	0.1585	44	1400	2100	1900	-	-
Nickel Catalyst	1.15	0.482	0	0.482	0	3250	5040	-	4830	0.341
Molecular Sieve 4A	0.965	0.69	0.27	0.42	4	5750	6550	5600	6190	0.411
Vycor glass	1.62	0.343	0.343	0	28	0	0	-	-	-

$(\bar{r}_a)_1$: obtained from eq. (32)

$(\bar{r}_a)_2$: obtained from eq. (31)

$(\bar{r}_a)_3$: obtained from $\frac{\Delta \varepsilon}{\Delta \log r}$ vs. r

$(\bar{r}_a)_4$: obtained from K_{eff} (eq. 38)

X: obtained from eqs. (39) and (28)

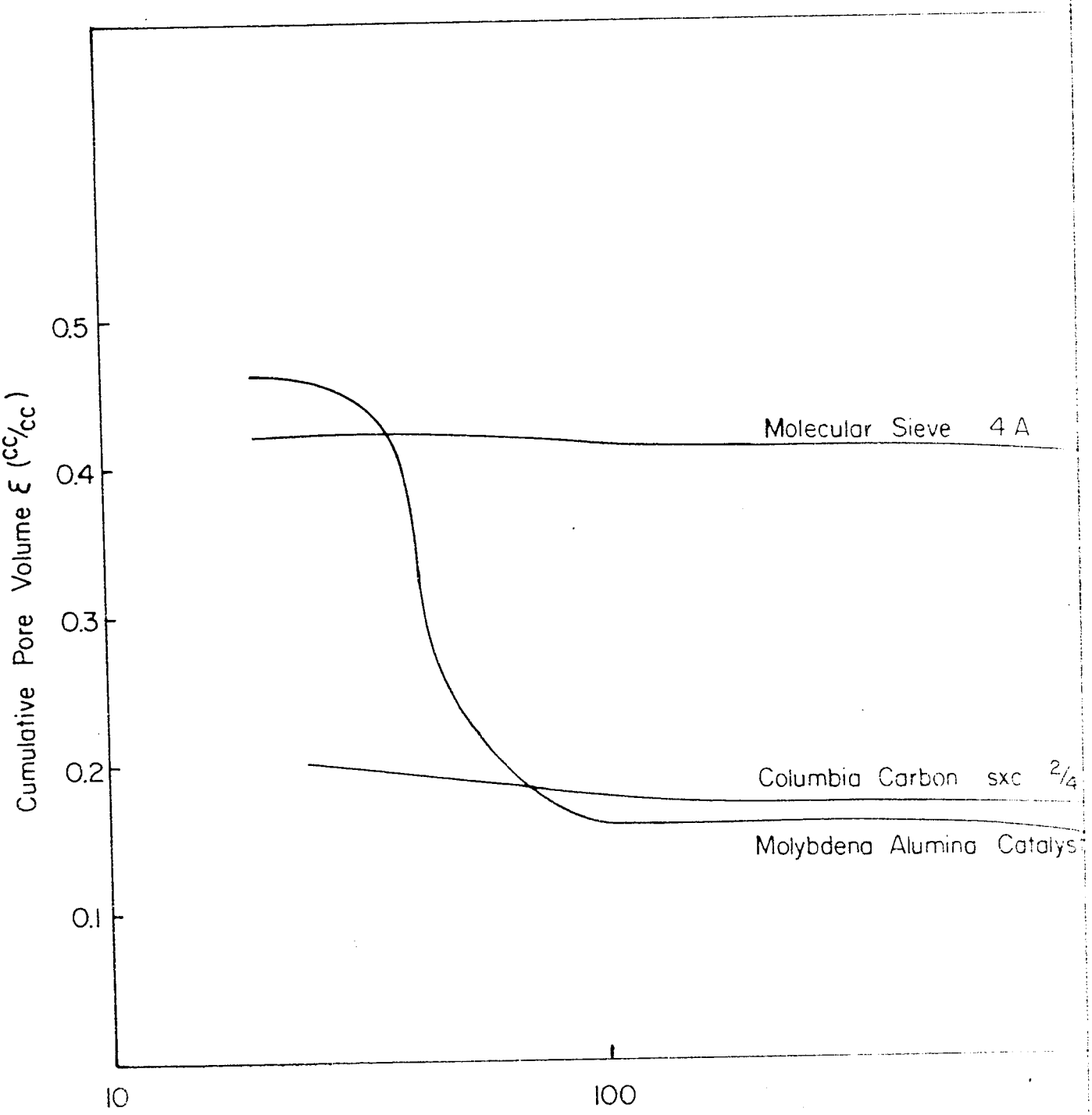

Fig. 3. Pore Size Distribution

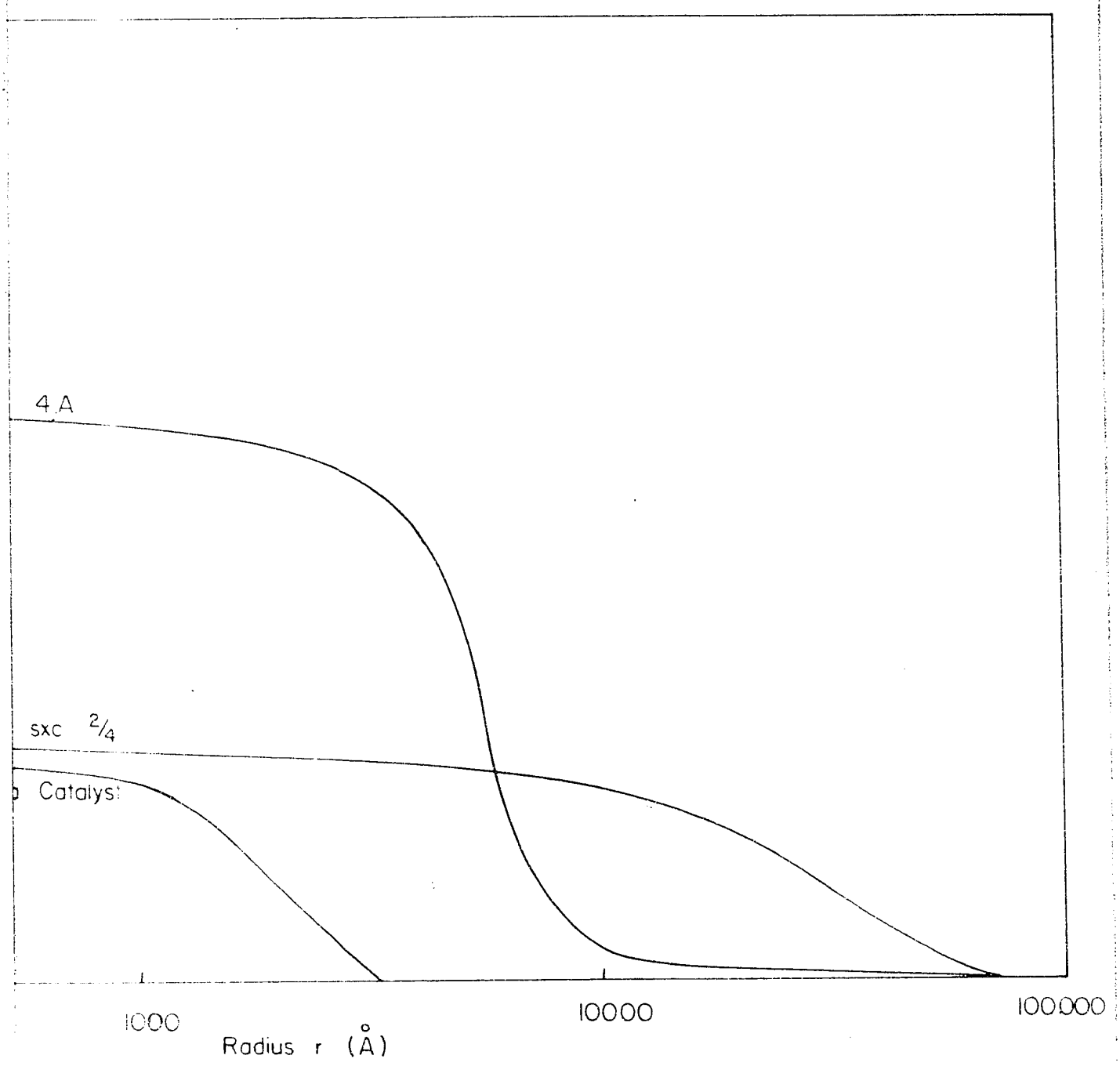

ribution

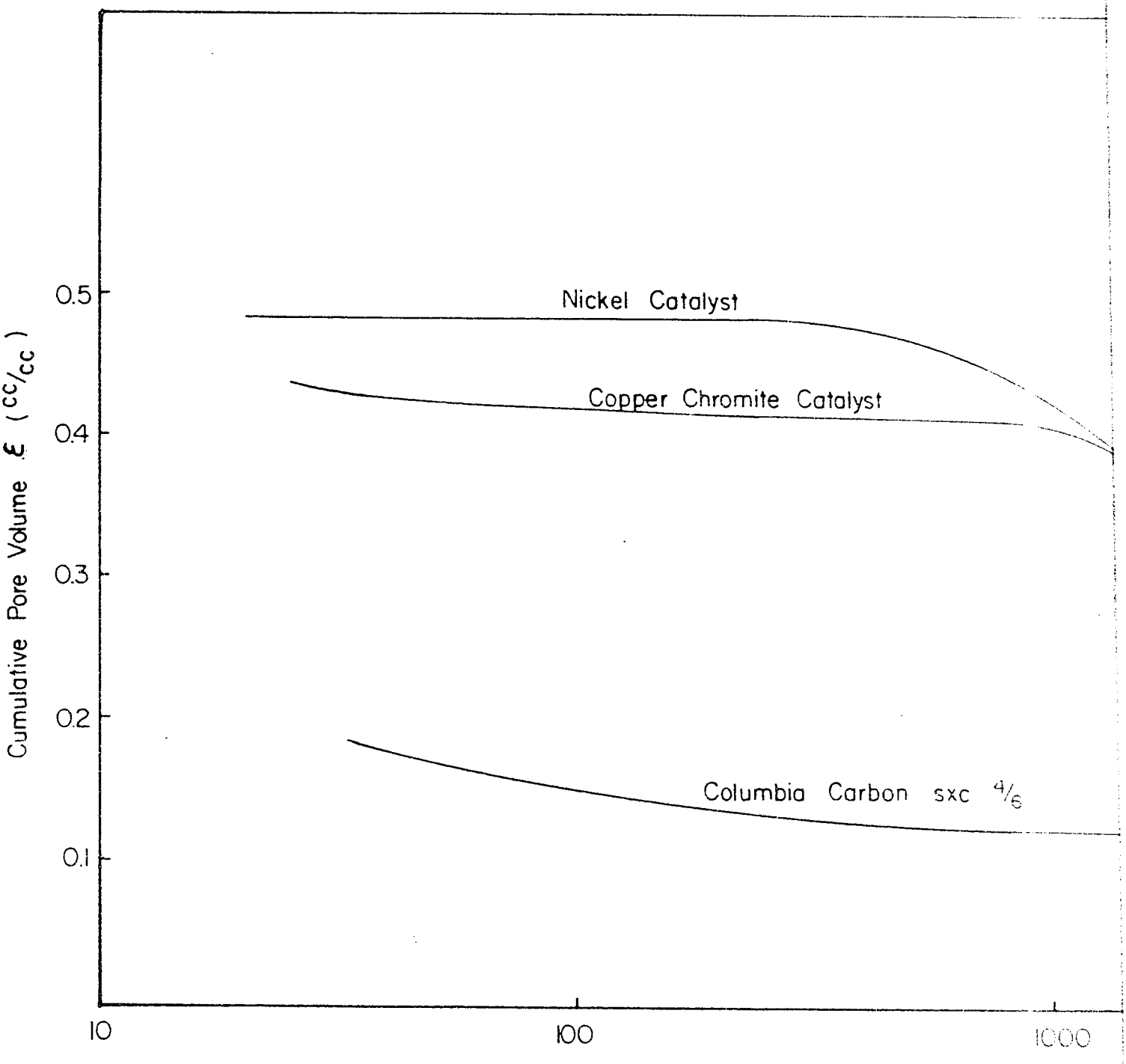

Fig. 4. Pore Size Distribution

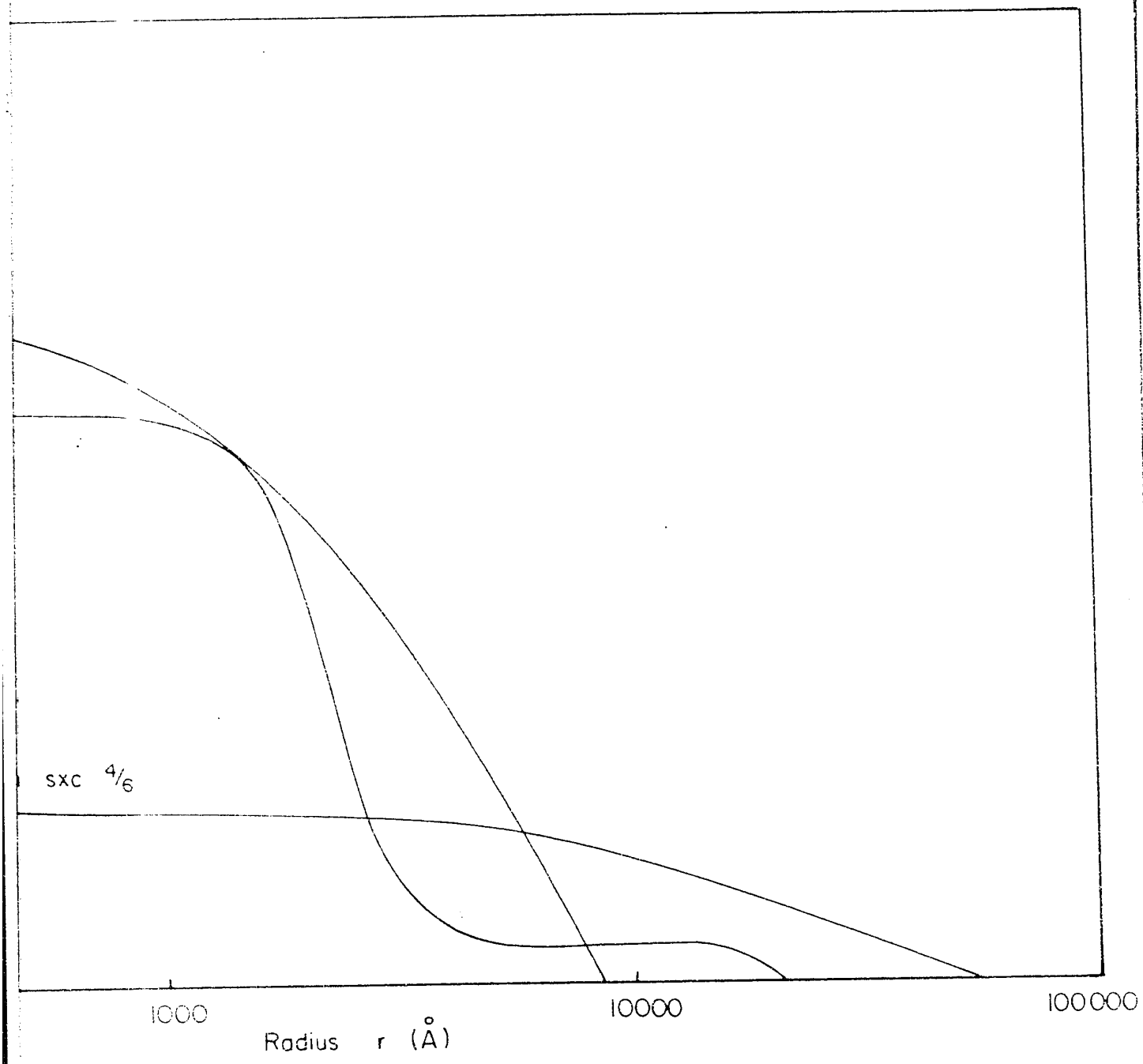

ution

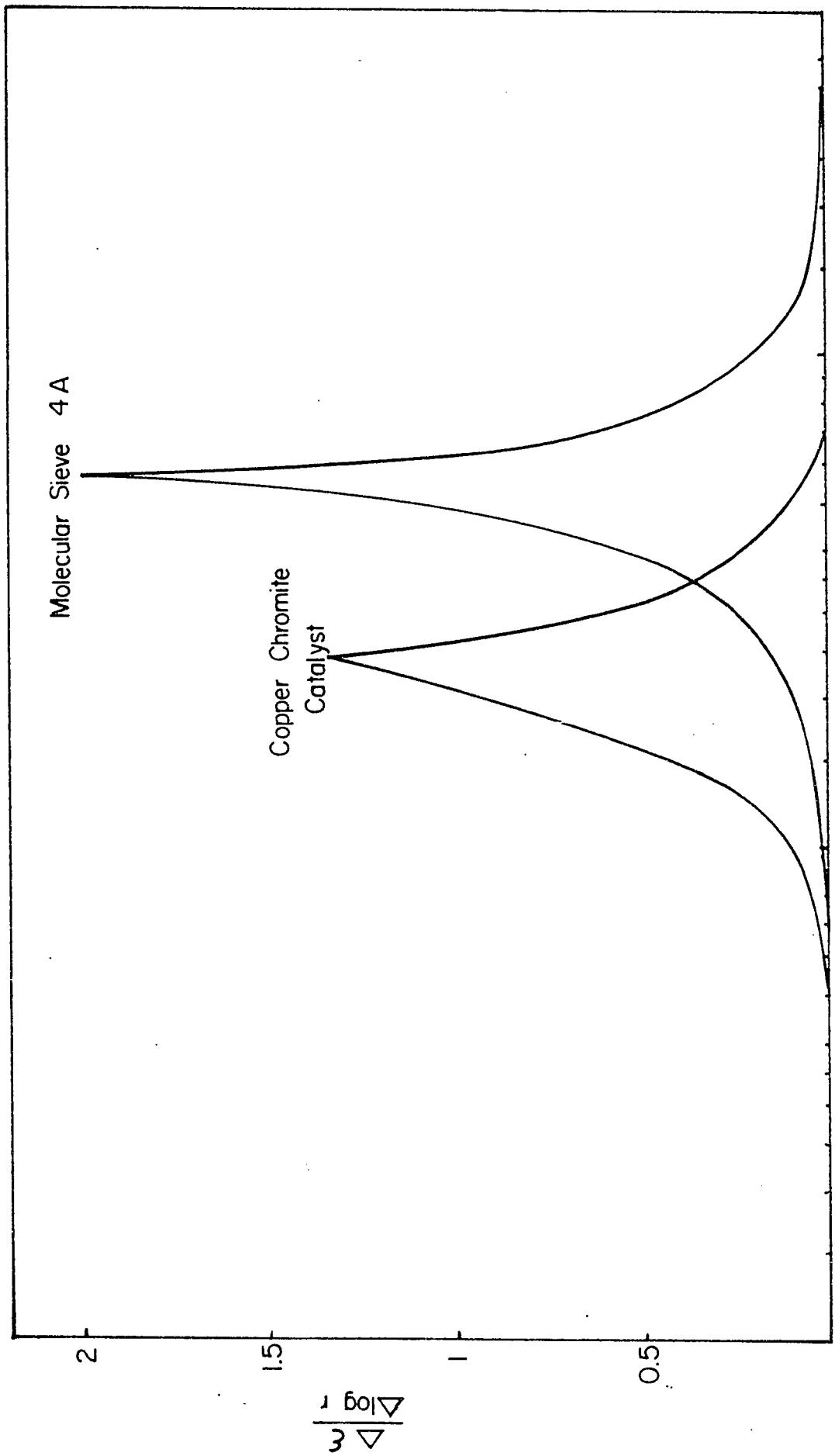

Fig. 5. Pore Size Distribution

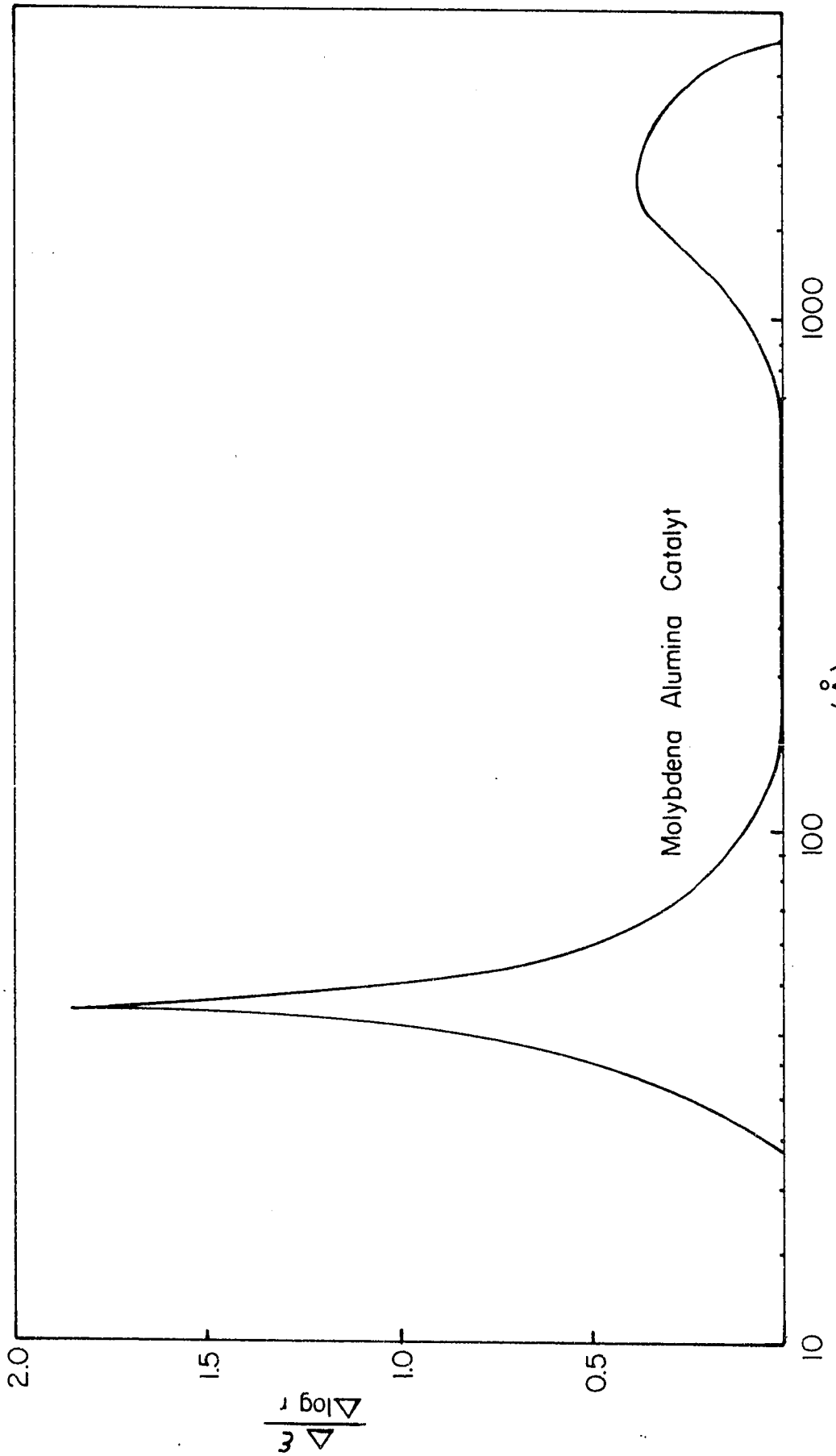

Fig. 6, Pore Size Distribution

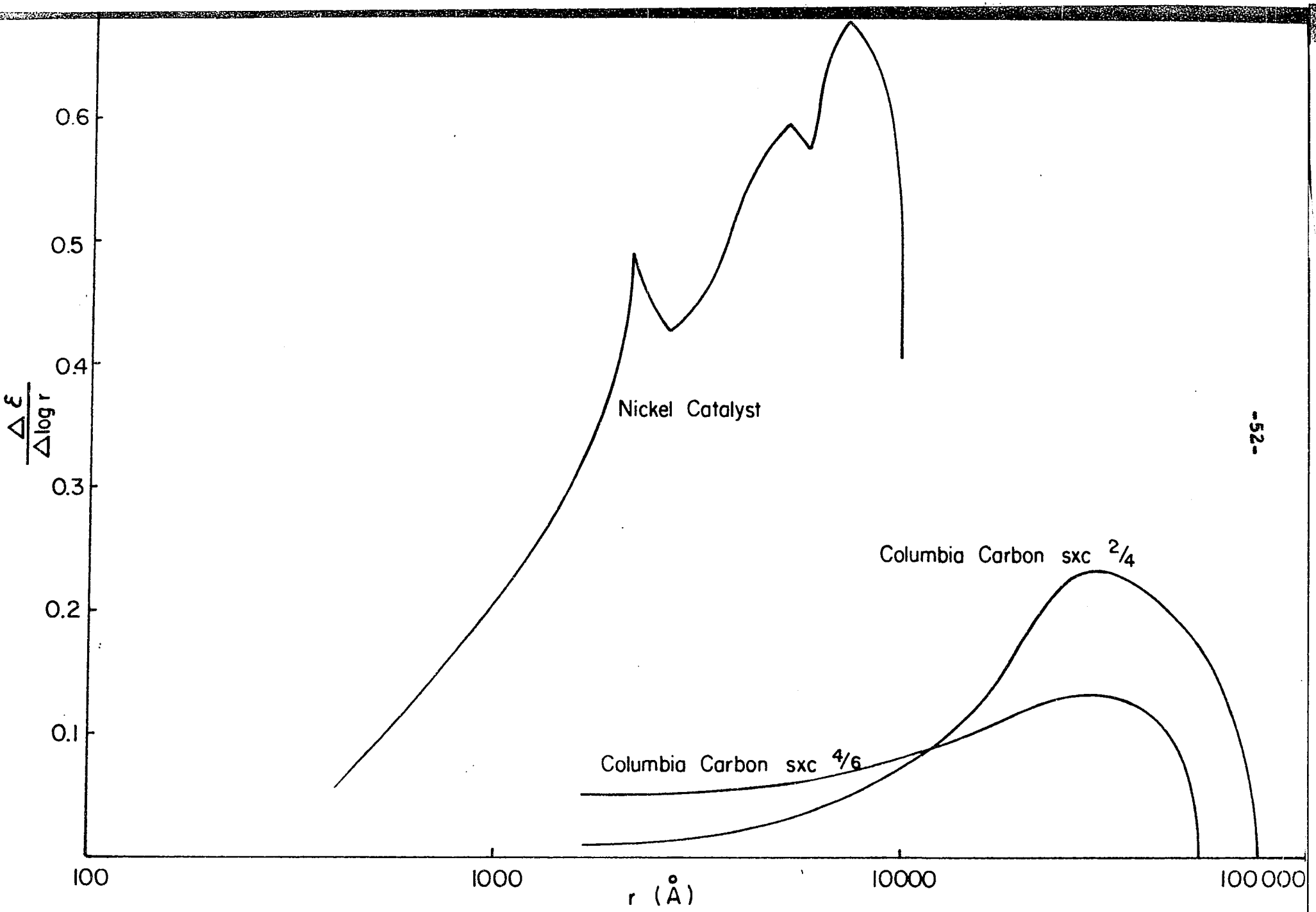

Fig. 7. Pore Size Distribution

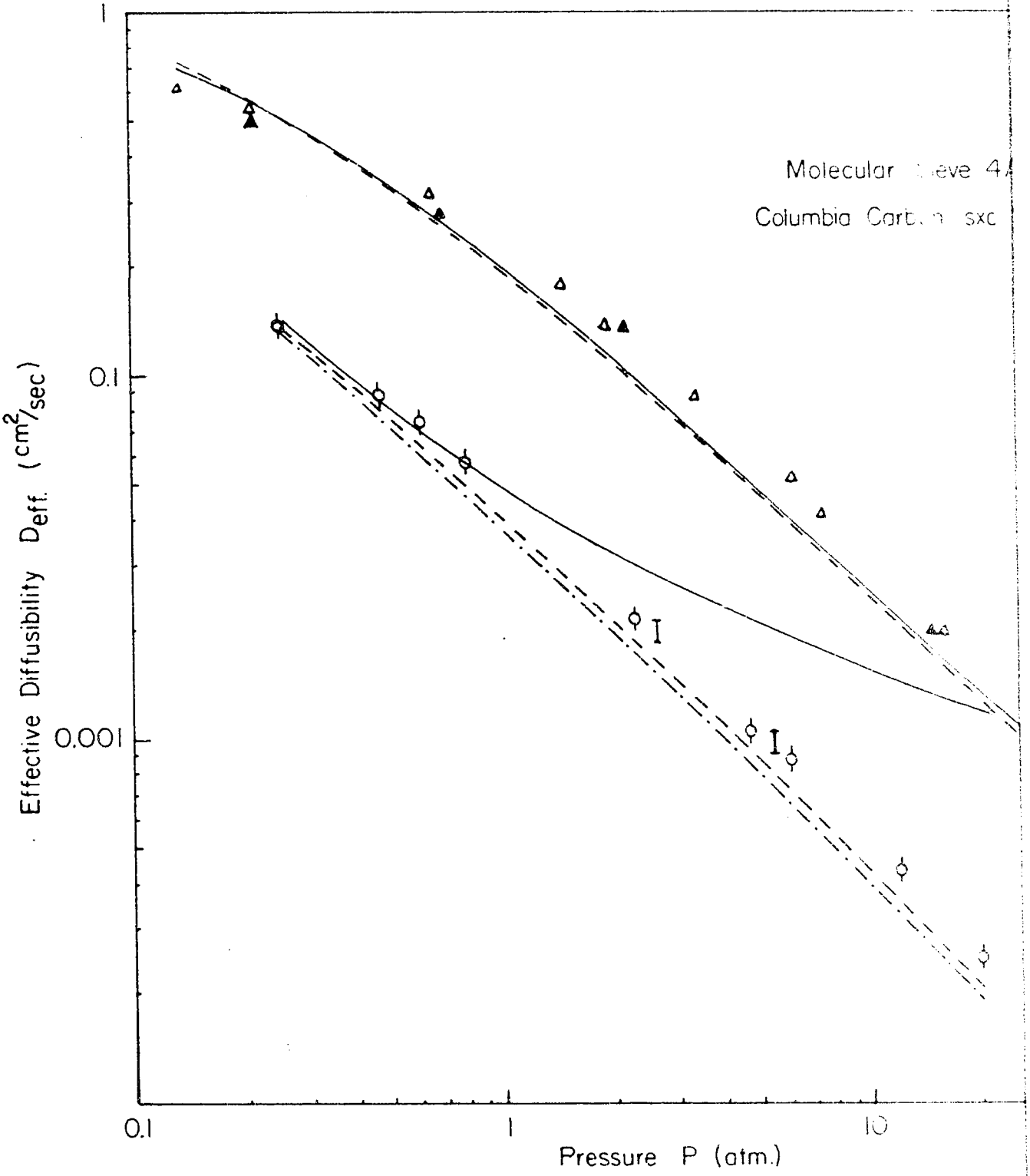

Fig. 8. Theoretical and Experimental Pellet Diffusivit
(-) Calculated from pore size distribution (e
(----) Calculated from experimental permeab
(-.-.-) Calculated from pore size distributio

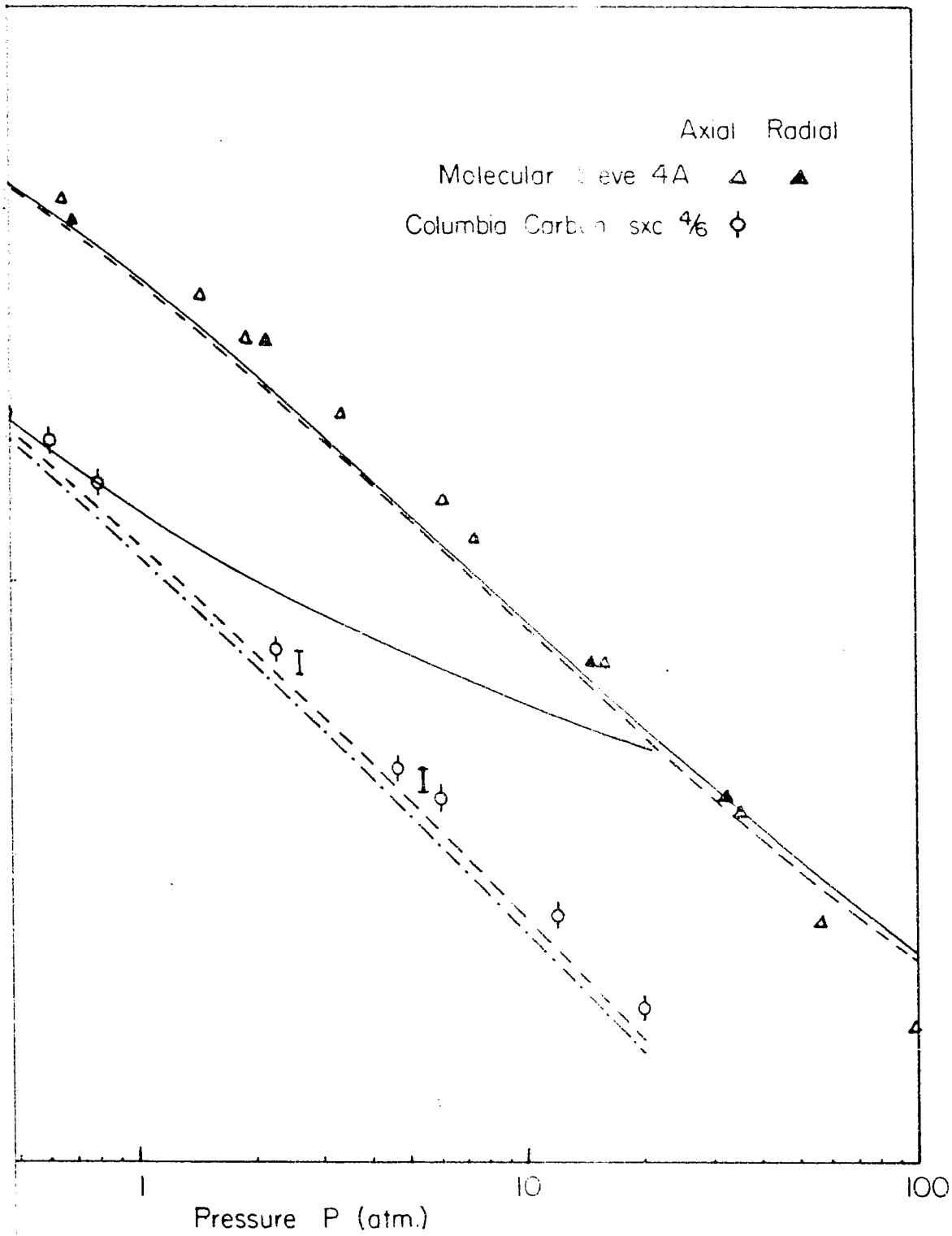

8. **Theoretical and Experimental Pellet Diffusivities**
   (-) Calculated from pore size distribution (eqs. 32, 28 and 12)
   (----) Calculated from experimental permeabilities (eqs. 38, 39 and 12)
   (-.-.-) Calculated from pore size distribution (for macropore contribution

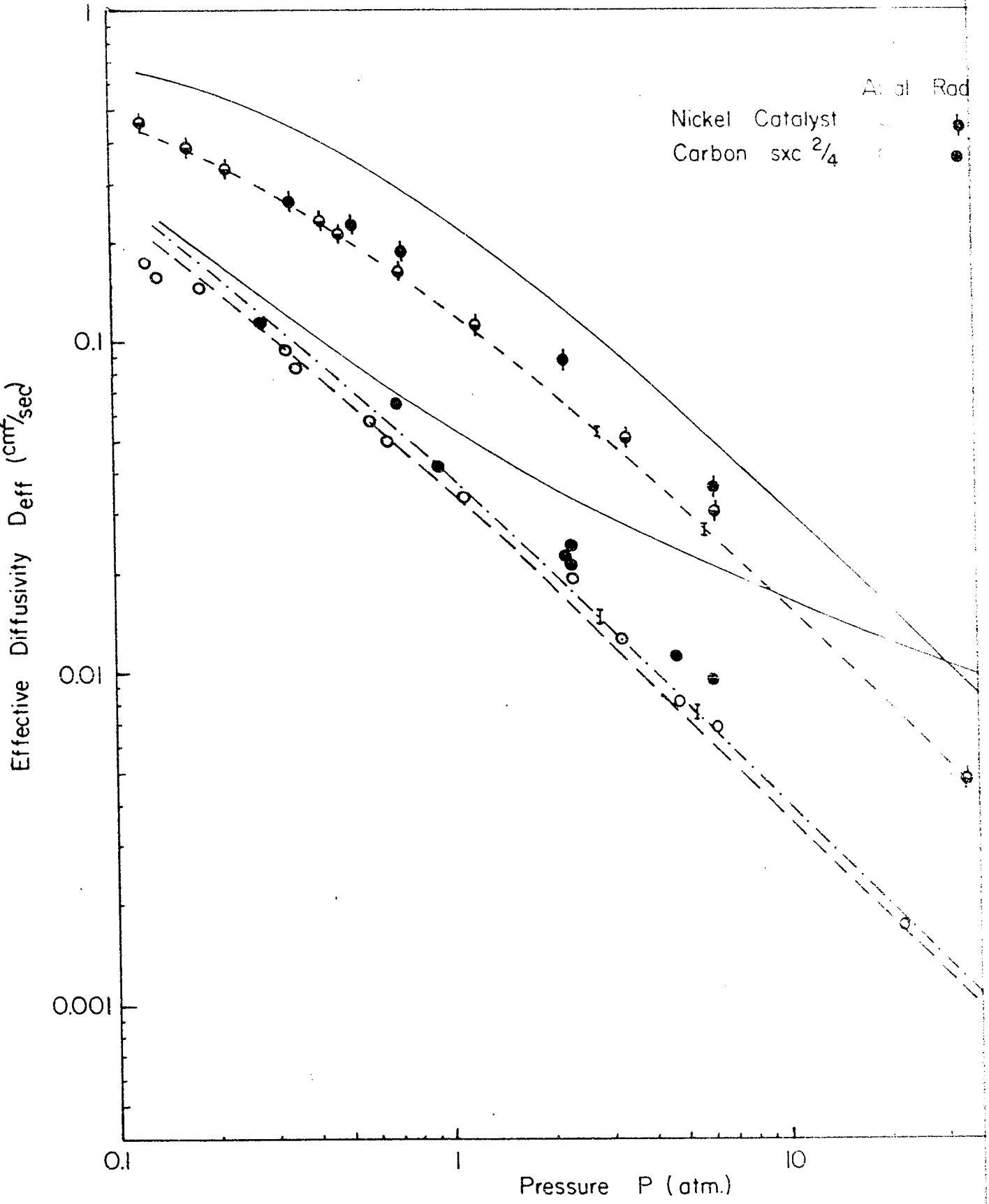

Fig. 9. Theoretical and Experimental Pellet Diffusivities
(-) Calculated from pore size distribution (eqs. 32, 28 and 12)
(----) Calculated from experimental permeabilities (eqs. 38, 39
(-.-.-) Calculated from pore size distribution (for macropore co

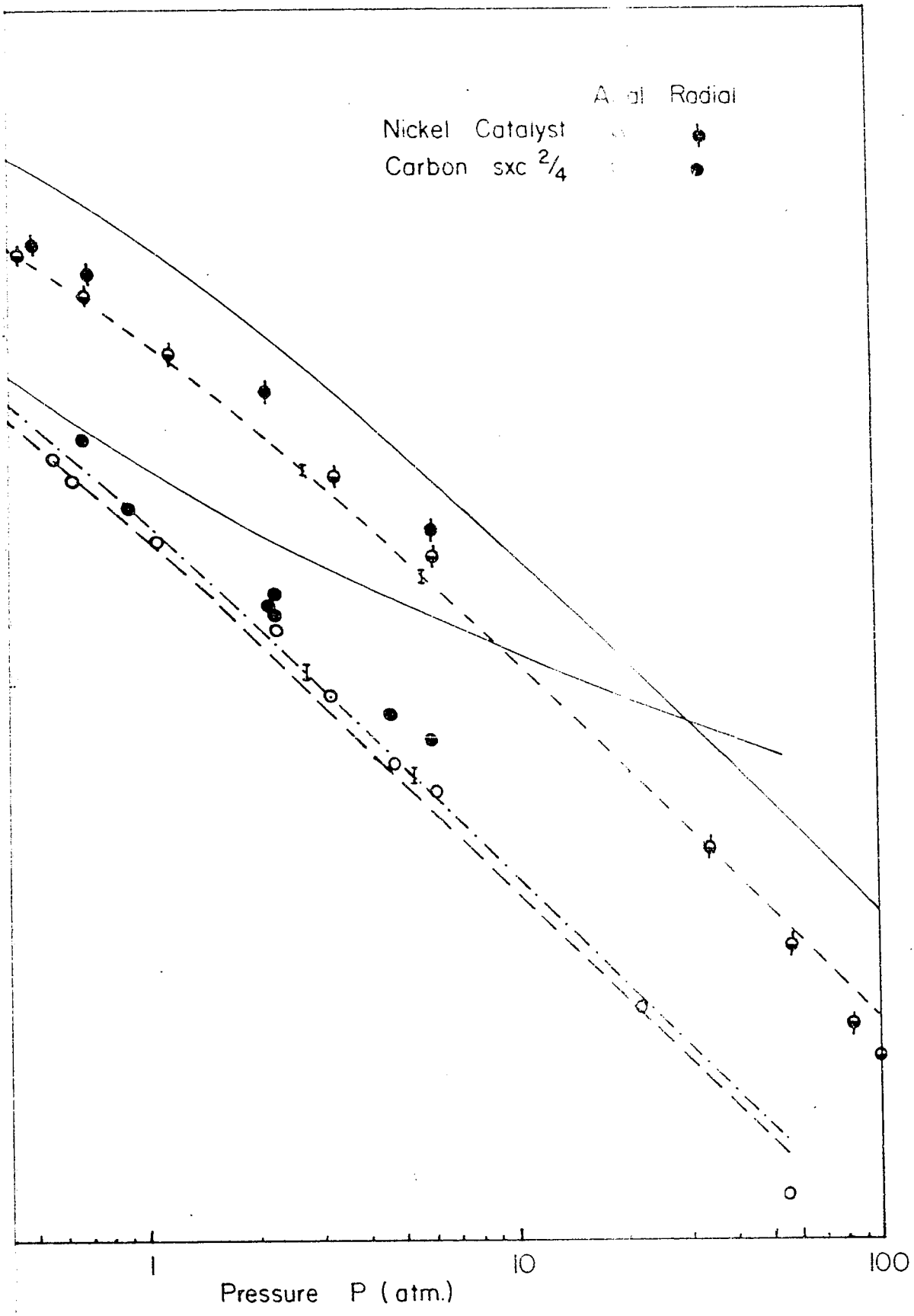

ical and Experimental Pellet Diffusivities
ılculated from pore size distribution (eqs. 32, 28 and 12)
Calculated from experimental permeabilities (eqs. 38, 39 and 12)
Calculated from pore size distribution (for macropore contribution only)

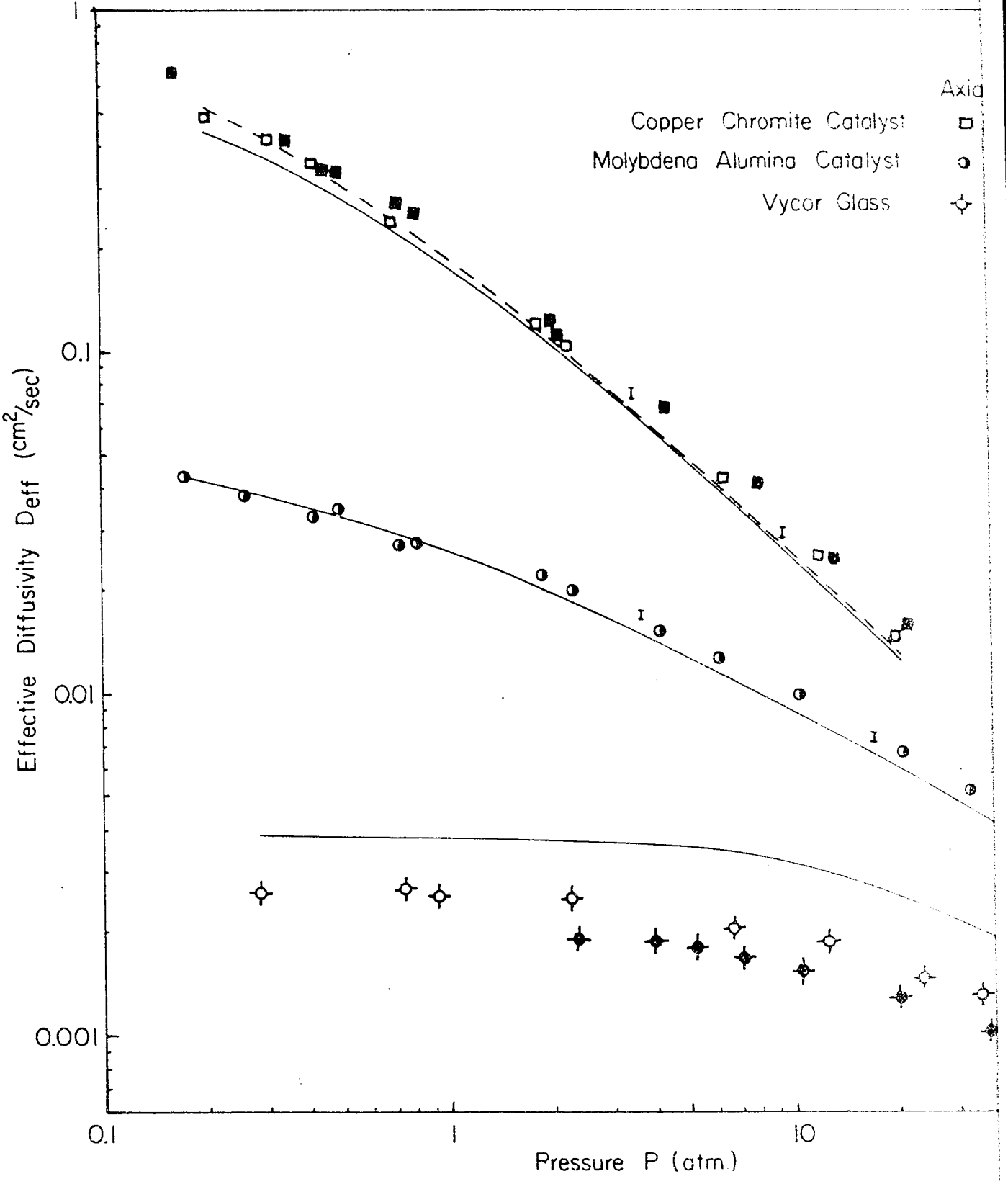

Fig. 10. Theoretical and Experimental Pellet Diffusivities
(-) Calculated from pore size distribution (eqs. 32, 28 and 12)
(----) Calculated from experimental permeabilities (eqs. 38, 39

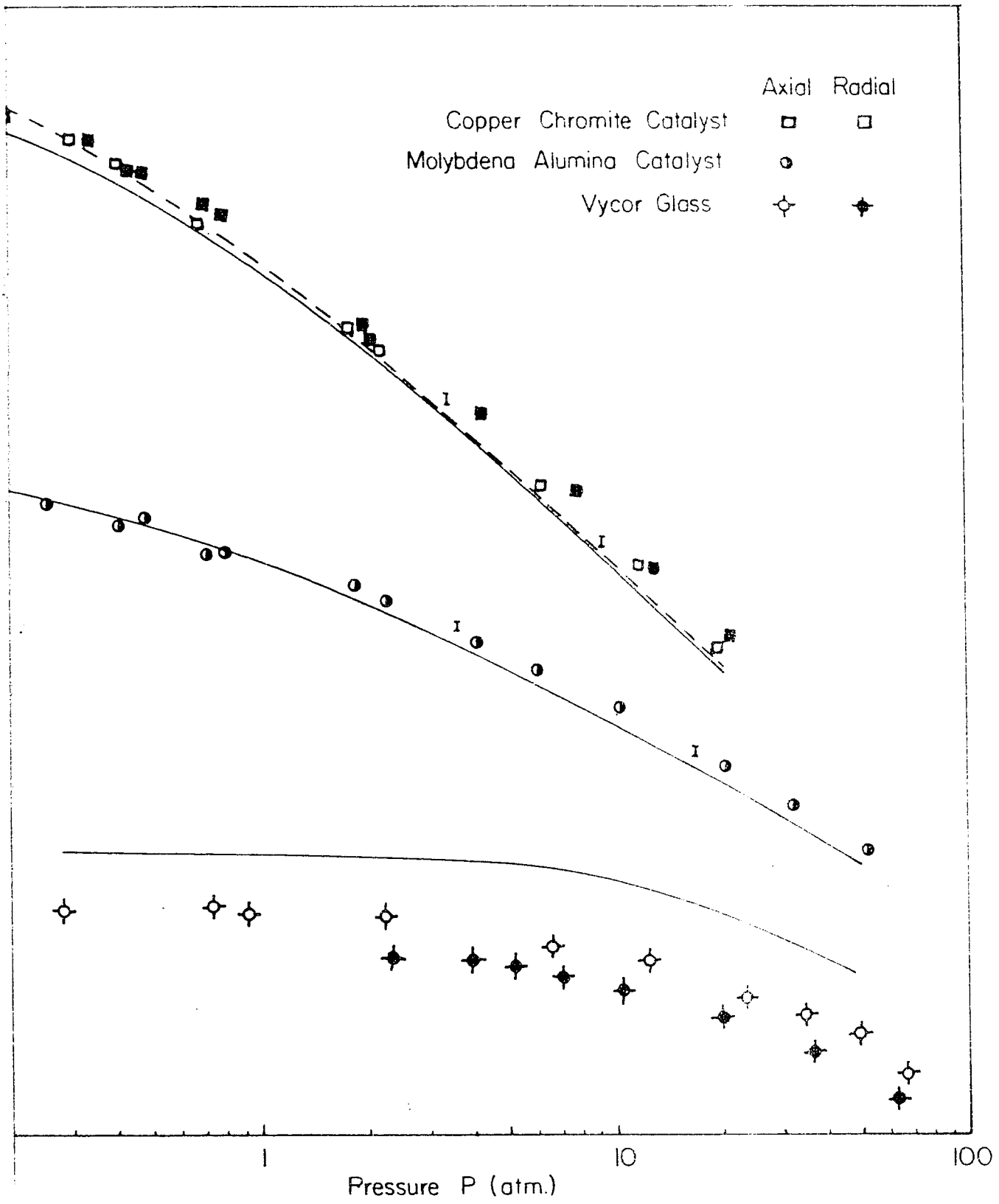

Theoretical and Experimental Pellet Diffusivities
(-) Calculated from pore size distribution (eqs. 32, 28 and 12)
(----) Calculated from experimental permeabilities (eqs. 38, 39 and 12)

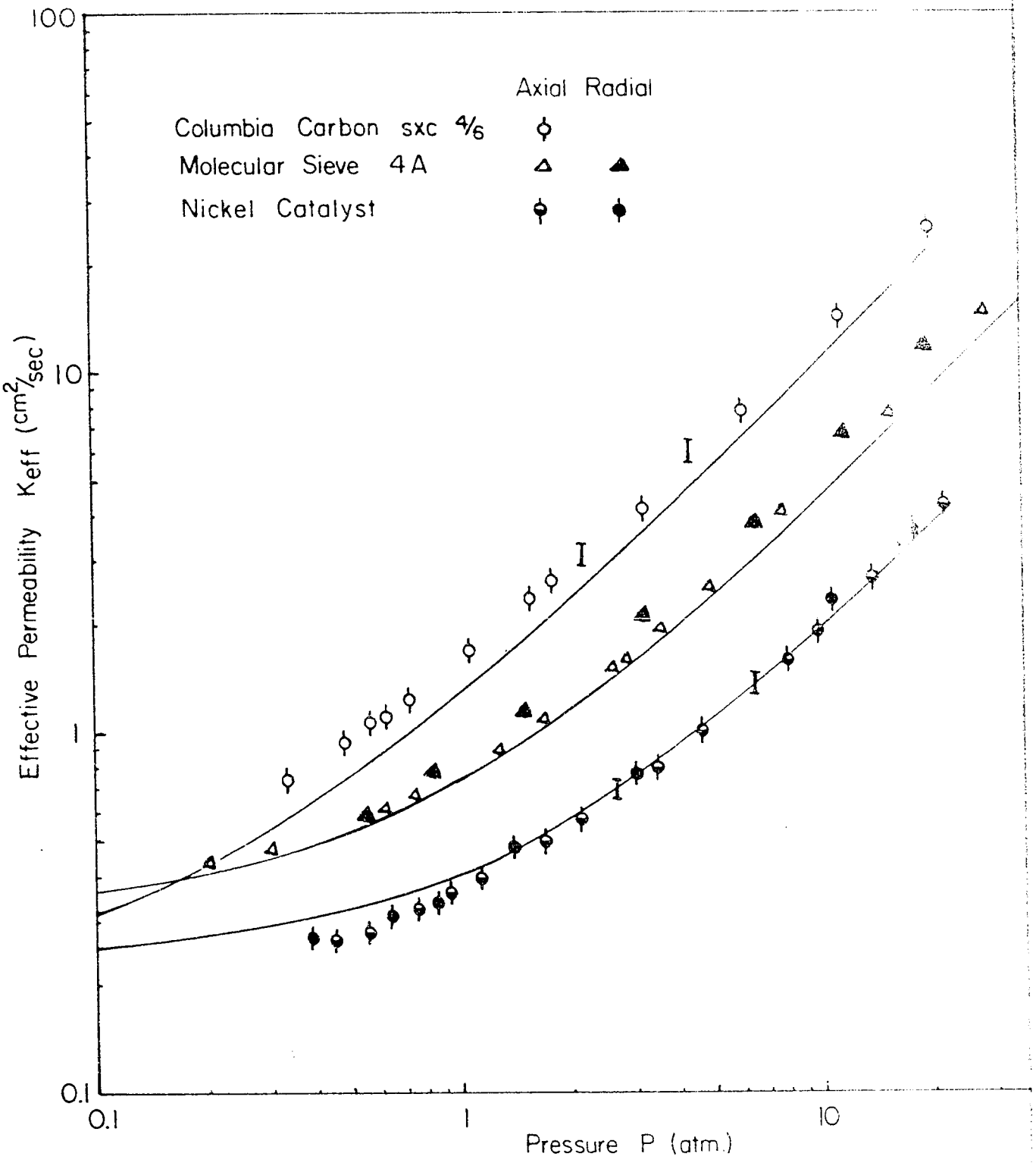

Fig. 11. Theoretical and Experimental Pellet Permeabilities
(-) Calculated from pore size distribution (eqs. 23, 28 and 32)

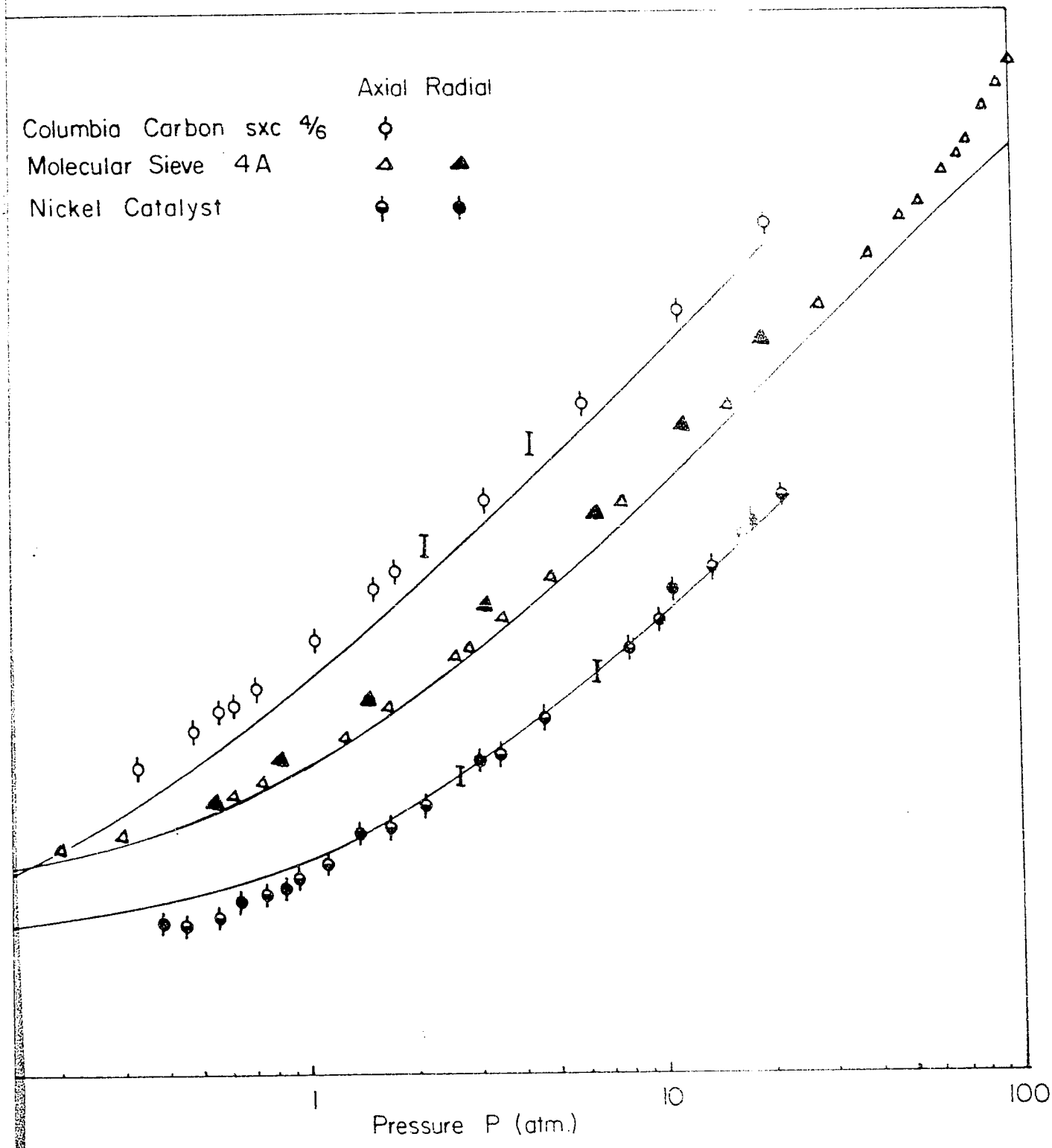

11. Theoretical and Experimental Pellet Permeabilities
(-) Calculated from pore size distribution (eqs. 23, 28 and 32)

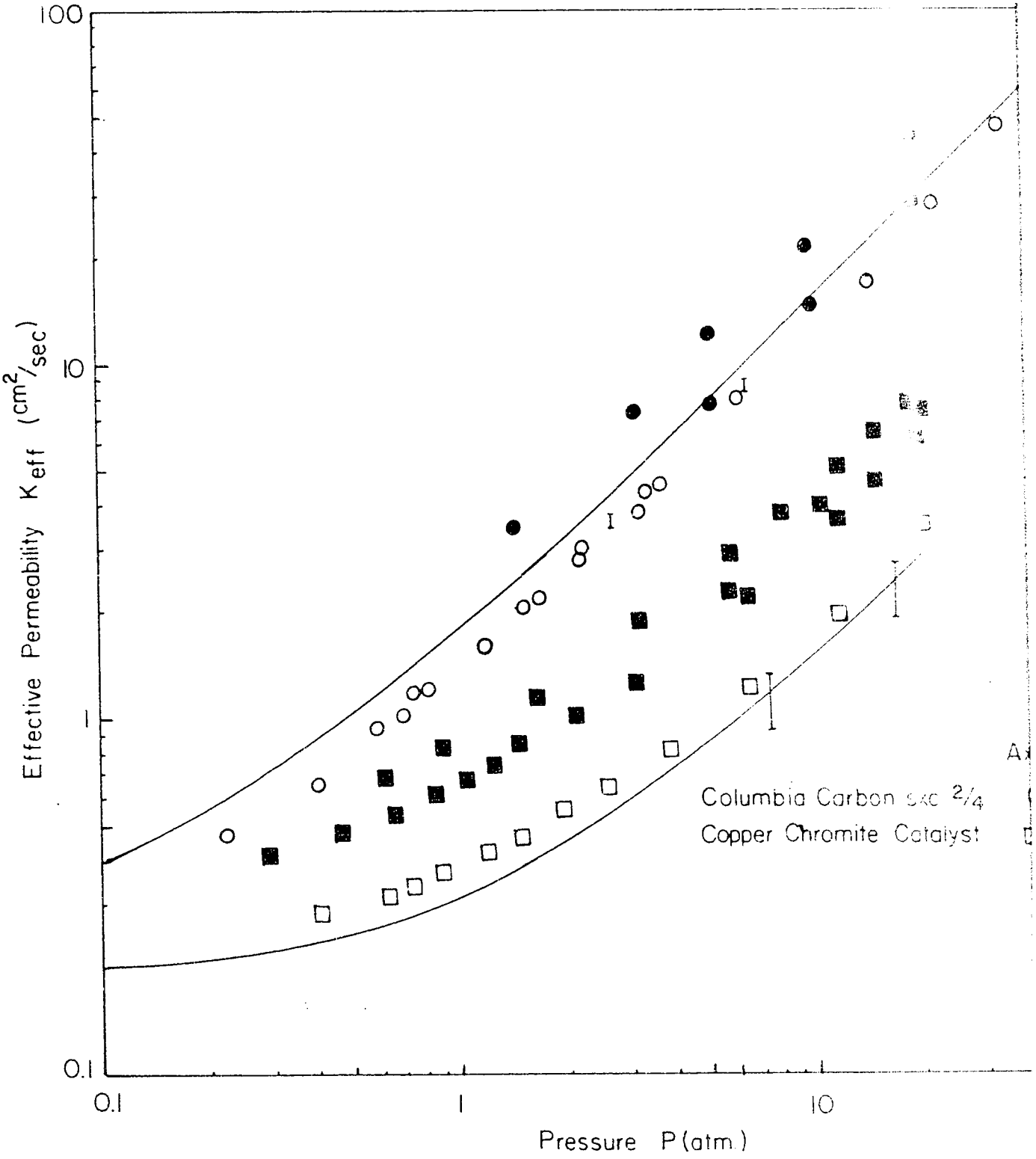

Fig. 12. Theoretical and Experimental Pellet Permeabilities
(-) Calculated from pore size distribution (eqs. 23, 28 and 32)

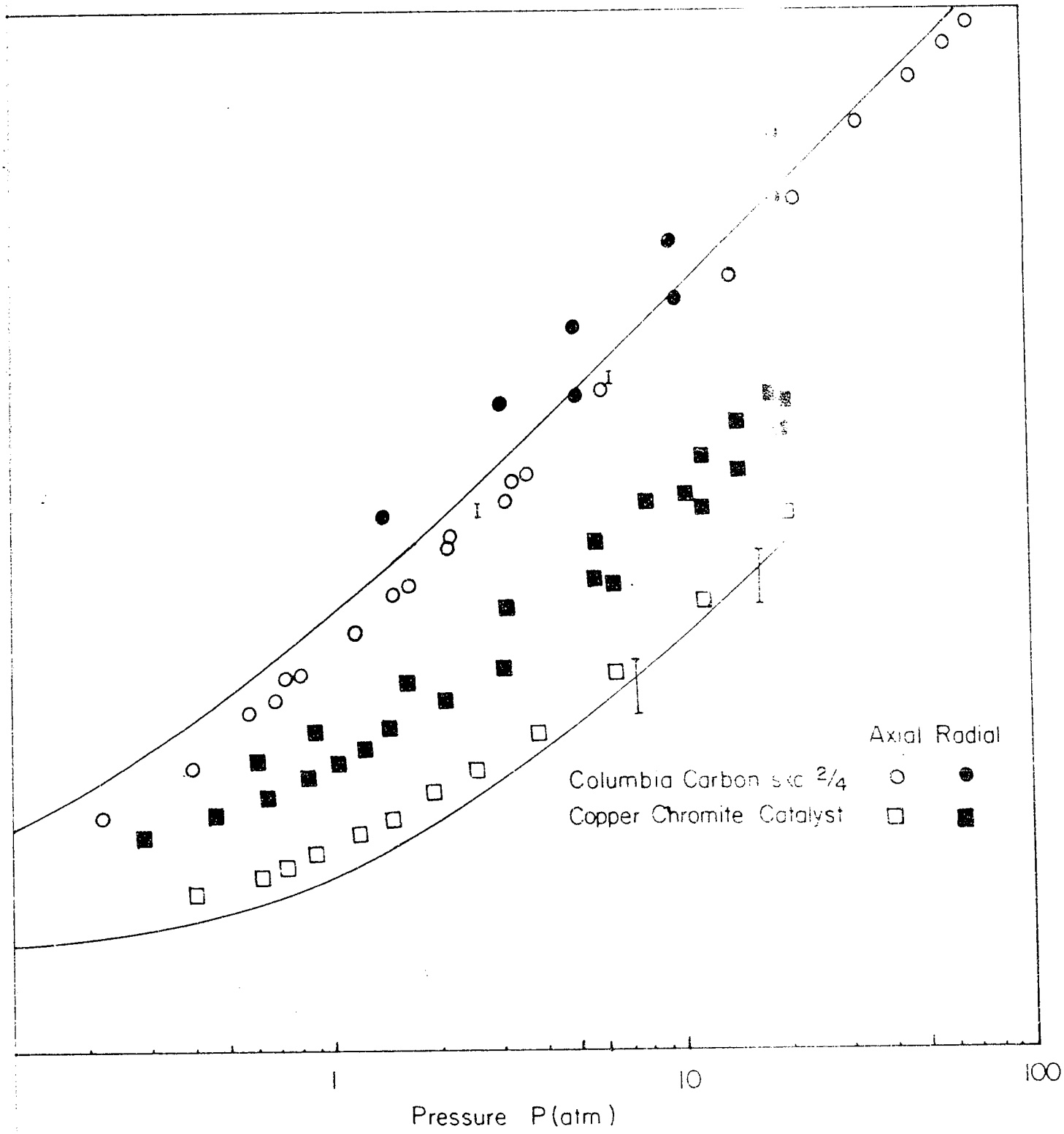

Fig. 12. Theoretical and Experimental Pellet Permeabilities
(-) Calculated from pore size distribution (eqs. 23, 28 and 32)

VI - DISCUSSION OF RESULTS

Diffusivity and permeability results obtained on seven materials over the pressure range 0.2 - 70 atm are shown in Fig. 8 - Fig. 12. Values calculated from equation (12) and equation (23) are identified as solid lines. The dashed lines represent the values of diffusivity calculated from permeability data by equations (38), (39) and (12). The measured axial and radial values are indicated by open and full symbols, respectively. Numerical values are given in Table 1 - Table 4. In the case of Vycor glass and the Molybdena Alumina Catalyst, only diffusivities were reported. The Mobil Durabead Cracking Catalyst (Socony Mobil Oil Co., Inc.) and silica gel pellets (Mobil Sorbead Desiccant, Socony Mobil Oil Co., Inc.) were also investigated. It was found that these materials have a small amount of macropores which were not detectable by mercury penetration, and therefore made correlation to pore structure impossible.

The theoretical and experimental diffusivity curves show the expected transition from Knudsen diffusion to bulk diffusion, the latter being inversely proportional to pressure. The results on Vycor glass and the Molybdena Alumina Catalyst show the characteristic levelling off to the pressure-independent Knudsen diffusion at subatmospheric pressures (Fig. 10). Pure Knudsen diffusion was not obtained on other materials at the subatmospheric pressure investigated (0.2 - 0.9 atm) because of the presence of large pore radii (3000 - 20,000 Å). The high values of K_{eff} of carbon pellets ($\varepsilon_a = 0.17$, $\bar{r}_a = 27,000$ Å) and the high values of D_{eff} of Copper Chromite Catalyst ($\varepsilon_a = 0.43$, $\bar{r}_a = 3200$ Å) obtained show the expected pore structure-dependent forced flow and diffusion. The former depends mainly on the pore reading and the latter depends on pore volume. The permeability curves show an

opposite trend as compared with the diffusivity curves in agreement with the theory. These opposite trends in diffusivities and permeability led to the difficulties in obtaining accurate high pressure diffusivity values. At pressure approaching zero, both the diffusivity and permeability curves come close to the same values indicating the relation $K_K = D_{KA}$.

To relate diffusivity and permeability to pore structure, the average pore radius $\bar{r}$ and the tortuosity X were evaluated from pore size distribution data. Wakao and Smith's method (23) was found to give the most satisfactory results. The equations used were

$$\bar{r} = \frac{\int r \, d\varepsilon}{\varepsilon} \tag{32}$$

$$X = \varepsilon \tag{28}$$

Diffusivities of porous materials were calculated by combining equations (32), (28) and (12). The calculated values agree satisfactorily with measured diffusivities except for the Nickel Catalyst and Vycor glass. The theoretical values for these materials are higher than the experimental values by a factor of 1.5. This may be due to the presence of blind pores. The other materials yield an average deviation of 10% and a maximum deviation of 20% between experimental and theoretical values.

By combining equations (32), (28) and (23), permeabilities of porous materials over a wide range of pressures were calculated. The calculated values give satisfactory agreement with experimental permeabilities. The maximum deviation between calculated and measured values is 20%. In the case of the Nickel Catalyst, the agreement is fortuitous due to a mutual cancellation of errors in the value of X and $\bar{r}$. This

method does not give very accurate results if a small amount of very large pores exist as in the case of Carbon pellets. It is obvious that the accuracy of the calculation depends mainly on the proper choice of $\bar{r}$.

Other methods, like those proposed by Marshall (11) and Millington and Quirk (13) were tested, but the results of diffusivity and permeability obtained were not satisfactory.

To relate D_{eff} and K_{eff}, the values of $\bar{r}$ and εX were evaluated from permeability measurements. Expressions relating $\bar{r}$ and εX to permeability data may be derived from the permeability equation given previously:

$$K_{eff} = \frac{2}{3} \bar{r} \bar{v} \varepsilon X \cdot \frac{\bar{r}^2 P \cdot \varphi}{8 \eta} \varepsilon X \qquad (23)$$

A plot of K_{eff} vs. P gives

$$\text{Intercept} = \frac{2}{3} \bar{r} \bar{v} \varepsilon X \qquad (36)$$

$$\text{Slope} = \frac{\bar{r}^2 \varphi \varepsilon X}{8 \eta} \qquad (37)$$

$$\frac{(36)}{(37)} \qquad \bar{r} = \frac{16 \eta \bar{v} \ \text{Slope}}{3 \varphi \ \text{Intercept}} \cdot 10^8 \ \text{Å} \qquad (38)$$

$$\frac{(37)}{(36)^2} \cdot \varepsilon X = \frac{9 \varphi \ (\text{Intercept})^2}{32 \eta \bar{v}^2 \ (\text{Slope})} \qquad (39)$$

The combination of equations (38), (39) and (12) permits the calculation of the effective diffusivity D_{eff} from permeability measurements. The values so calculated give good agreement with measured diffusivities. The average and maximum deviation between calculated and measured values are 10% and 20% respectively. Since the value of εX can be estimated from permeability data alone, the prediction of D_{eff} from K_{eff} requires no additional data, but is limited to uni-disperse media (eq. 11). This method appears to solve the problem of blind pores as well as other effects as justified by the good results obtained with the Nickel Catalyst. Therefore, it is more reliable to predict D_{eff} from K_{eff} than from pore size distribution. It may be pointed out that permeability measurements can be made more readily than diffusion measurements.

The theory of Wakao and Smith (23) regarding the contributions for diffusion through various pores has been verified on various types of material and extended to a wider pressure range than before. Their theory seems to apply to most of the uni-disperse and bi-disperse media, but does not apply to the Nickel Catalyst and Vycor glass which were not pelleted.

Particular attention was given to micropore contribution to diffusion at high pressures for materials having a large amount of micropore volume. In the investigation of Carbon SXC 2/4, and Carbon SXC 4/6 ($\varepsilon_i = 0.62$, $\varepsilon_a = 0.17$), it was found that only the macropore volumes serve as channels for diffusion, and the large amount of micropore volume was believed to consist of blind pores. In the case of a Molybdena Alumina Catalyst ($\varepsilon_i = 0.3025$, $\varepsilon_a = 0.1585$), the entire micropore volume contributes to diffusion.

In the case of Vycor glass ($\varepsilon_i = 0.343$, $\varepsilon_a = 0$), diffusion measurements provide a means of investigating the pore structure more

fully than in other materials since it contains only micropores of narrow size distribution. Sorption isotherms of various gases on Vycor glass are reported by Amberg and McIntosh (1) and Barrer and Barrie (2). These authors were able to calculate a Kelvin radius of about 28 Å and a B. E. T. surface area of about 119 m^2/g from the desorption branch of hysteresis loop.

The diffusion measurements made in the range 0.3 - 70 atm cover the range of Knudsen ($<$ 3 atm), of transition (3-20 atm) and of bulk diffusion ($>$ 20 atm). The controlling pore radius for this material can be calculated by applying the measured diffusivities to the Knudsen (equation 9) and the transition regions (equation 11). The value so calculated was 28 Å $\pm$ 2, in agreement with the desorption Kelvin radius obtained by Amberg et al (1) and Barrer et al (2). The tortuosity X obtained from equation (9) was 0.23, compared to Barrer and Barrie's value of 0.18. In order to determine whether the low value of X was due to a lamellar structure in Vycor glass, diffusion measurements were performed along an axis perpendicular to the one used originally (i.e. radial diffusion). The values found were only 20% lower. This result justifies the assumption of random orientation of pores. For lack of a better value, the tortuous path value of $\frac{1}{\sqrt{2}}$ proposed by Wheeler (24) was used.

From the sorption isotherms reported by Amberg et al (1), the pore geometry of Vycor glass seems to conform to de Boer's shape group XV (7) consisting of cylindrical sections and globular enlargements. By assuming a pore model of R_c (radius of constriction) = 28 Å

R_g (radius of globular enlargements) = 2 R_c

L_c (length of constriction) = 50 Å

and the tortuous path value of $\frac{1}{\sqrt{2}}$, good agreement between the calculated and measured values of diffusivities and surface area was obtained.

It is therefore concluded that a reasonable pore model of Vycor glass (3) comprises periodic constrictions (R_c = 28 Å) and globular enlargements (R_s = 2 R_c) as well as an unknown amount of blind pores.

The diffusivity and permeability measurements along axial and radial directions of cylindrical pellets may serve to determine the isotropy of pore properties. The average deviation between the axial and radial values obtained were as follows:

Pellets	Average deviation between axial and radial	
	% D_{eff}	% K_{eff}
Carbon SXC 2/4	22	35
Copper Chromite Catalyst	5	46
Molecular Sieve 4A	5	7
Nickel Catalyst	12	5
Vycor glass	20	

Diffusivities and permeabilities of Carbon and permeabilities of Copper Chromite Catalyst obtained in the radial direction are higher than those obtained in the axial direction. The other materials appear to have approximately the same pore properties in both directions. The investigation on "pellet to pellet variation" shows that the pore properties in the axial are more uniform than those in the radial direction. In the case of Copper Chromite pellets, "pellet to pellet variation" was observed in both axial and radial forced flow, but not in diffusion. These results provide evidence that Copper Chromite pellets contain the same free crossectional area, but differ in average pore size along the two directions investigated.

Pore radii obtained by various methods are shown in Table 6. The method of Wakao and Smith (23) leads to an incorrect estimation when there is overlap between the micropore and the macropore regions. Marshall's method for calculating $\bar{r}$ from equation (31) seems to put too much weight on the large pores. In the micropore region, distribution plots show sharp peaks and therefore the value obtained from these curves represents a good average of the radius. However, a sharp peak of normal distribution does not always exist in the macropore region as seen from the study of the materials in this project and the data reported by Mischke et al (4) and Robertson et al (17). The values of $\bar{r}$ obtained from K_{eff} by applying eq. (38) seems to yield a good average radius in every case. Therefore, it is reliable and convenient to calculate $\bar{r}$ from K_{eff} especially for materials having a small amount of very large pores which can not be detected accurately by mercury penetration, and for those having blind pores.

VII - CONCLUSIONS

1. Wakao and Smith's method predicts reliable effective diffusivities for pelleted materials when the micropore contribution is known.

2. For other materials which are not pelleted and for those which contain blind pores, effective diffusivities can be predicted from permeability measurements. This further supports that diffusivity measurements can be replaced by permeability measurements which can be made more readily.

3. The combination of equations (28), (32) and (23) predicts reliable effective permeabilities over a wide range of pressures.

4. Diffusivity measurements over a wide pressure range yield the controlling pore radius for micropore solids and can therefore be used for investigating the pore structure of Vycor glass.

5. Axial and radial diffusivity and permeability measurements provide a means of investigating the isotropy of the pore structure.

VIII - ACKNOWLEDGEMENTS

The author is deeply indebted to Dr. D. Basmadjian for his prudent guidance and enthusiastic encouragement in carrying out this work, and for his advice and help in preparing this thesis.

Thanks are given to the Fuels Division, Mines Branch, Department of Mines and Technical Surveys, Ottawa, for measuring the pore size distribution of the materials and the use of their facilities in preparing the sample pellets, and to the graduate students of the Chemical Engineering Department for their many suggestions and the reading of the manuscripts.

The financial support of the National Research Council of Canada, Ottawa, is greatly appreciated.

IX - NOMENCLATURE

A	=	geometric area of porous sample	cm^2
D	=	diffusivity	cm^2/sec
D_{AB}	=	binary bulk or ordinary diffusivity for system A-B	cm^2/sec
D_{KA}	=	Knudsen diffusivity of gas A	cm^2/sec
$\bar{D}_{K_a}$	=	mean Knudsen diffusivity of gas A in the macropores	cm^2/sec
$\bar{D}_{K_i}$	=	mean Knudsen diffusivity of gas A in the micropores	cm^2/sec
D_{eff}	=	effective diffusivity	cm^2/sec
K	=	permeability	cm^2/sec
K_K	=	Knudsen permeability	cm^2/sec
K_p	=	Poiseuille permeability	cm^2/sec
K'	=	permeability	cm^2
K_{eff}	=	effective permeability	cm^2/sec
k_o	=	shape factor	dimensionless
L	=	length of porous sample	cm
L'	=	length of flow path	cm
M	=	molecular weight	g/g mole
N_A	=	molar transport rate of gas A	g mole/(cm^2)(sec)
P	=	total pressure	atm
Q	=	volumetric flow rate	cm^3/sec

R	=	gas constant	$(cm^3)(atm)/(°K)(g\ mole)$
r	=	pore radius	Å
$\bar{r}_a$	=	average macropore radius	Å
$\bar{r}_i$	=	average micropore radius	Å
r_h	=	hydraulic radius	Å
S	=	surface area of porous media	cm^2/g
T	=	temperature	°K
$\bar{v}$	=	average molecular velocity	cm/sec
X	=	tortuosity	dimensionless
y_A	=	mole fraction of gas A	dimensionless
z	=	distance in the direction of flow	cm

Greek letters

ε	=	porosity	cm^3/cm^3
ε_a	=	macropore volume	cm^3/cm^3
ε_i	=	micropore volume	cm^3/cm^3
α	=	ratio of diffusion rates $1 \cdot \frac{N_B}{N_A}$	dimensionless
ρ	=	gas density	g/cm^3
η	=	gas viscosity	dyne-sec/cm^2
φ	=	conversion factor, 1.013×10^6	dynes-sec/atm-cm^2
λ	=	mean free path	Å

Subscripts

a, i	=	macropore and micropore, respectively
A, B	=	hydrogen and nitrogen, respectively
1, 2	=	hydrogen and nitrogen sides of pellet

X - REFERENCES

1. Amberg, C.H., and McIntosh, R., Can. J. Chem. 30, 1012 (1952).
2. Barrer, R.M., and Barrie, J.A., Proc. Roy. Soc. A, 213, 250 (1952).
3. Basmadjian, D. and Chu, K.P., "On the Pore Structure of Vycor Glass", submitted for publication to Can. J. Chem.
4. Buckingham, E., Bulletin No. 25, U.S. Dept. of Agriculture, Bureau of Soils (1904).
5. Carman, P.C., "Flow of Gases through Porous Media", Butterworths, Scientific Publications, London (1956).
6. Dacey, J.R. and Fendley, J.A., Proceedings of the Tenth Symposium of the Colston Research Society, "The Structure and Properties of Porous Materials", p. 142, Butterworths, Scientific Publications, London (1958).
7. de Boer, J.H., Proceedings of the Tenth Symposium of the Colston Research Society, "The Structure and Properties of Porous Materials", p. 68, Butterworths, Scientific Publications, London (1958).
8. Hoogschagen, J., Ind. Eng. Chem., 47, 906 (1955).
9. Klinkenberg, L.J., Bull. geol. Soc. Amer., 62, 559 (1951).
10. Lea, F.M., and Nurse, R.W., J. Soc. Chem. Ind., London (Trans), 58, 277 (1939).
11. Marshall, T.J., J. Soil. Sci., 9, No. 1, 1 (1958).
12. Masamune, S., and Smith, J.M., A.I.Ch.E. Journal, 8, 217 (1962).
13. Millington, R.J., and Quirk, J.P., Trans. Faraday Soc. 57, 1200 (1961).
14. Mischke, R.A., and Smith, J.M., I.E.C. Fundamentals, 1, 288 (1962).
15. Pollard, W.G. and Present, R.D., Phys. Rev., 73, 762 (1948).
16. Ritter, L.C. and Drake, R.L., Ind. Eng. Chem., An. Ed., 17, 782 (1945).

17. Robertson, J.L. and Smith, J.M., A.I.Ch.E. Journal, 9, 342 (1963).

18. Rothfeld, L.B., Ph.D. Thesis, Univ. of Wisconsin, Madison, Wisconsin (1961).

19. Rothfeld, L.B., A.I.Ch.E. Journal, 9, 19 (1963).

20. Scott, D.S. and Dullien, F.A.L., A.I.Ch.E. Journal, 8, 113 (1962).

21. Smith, J.M., "Chemical Engineering Kinetics", McGraw-Hill Book Company, Inc., N.Y. (1956).

22. Treybal, R.E., "Mass Transfer Operations", McGraw-Hill Book Company, Inc., N.Y. (1955).

23. Wakao, N. and Smith, J.M., Chem. Eng. Science, 17, 828 (1962).

24. Wheeler, A., "Advances in Catalysis", Vol. 3, p. 249, Academic Press, N.Y. (1951).

25. Wicke, E. and Kallenbach, R., Kolloid Z., 97, 135 (1941).

26. The Fuels Division, Mines Branch, Department of Mines and Technical Surveys, Ottawa.

27. Perry, J.H., "Chemical Engineers' Handbook", 3rd Edition, McGraw-Hill Book Company, Inc., N.Y. (1950).

XI - APPENDIX: SAMPLE CALCULATIONS

A. The calculation of D_{eff} from diffusion measurement.

Molecular Sieve 4A

$P = 0.664$ atm

$Q = 4.13\ cm^3/sec$ = volumetric flow rate of the nitrogen stream ($M_2 + N_2$)

$y_{A_2} = 0.040$

$$N_A = \frac{Q}{A} \cdot \rho \cdot y_{A_2} = \frac{Q}{A} \cdot \frac{P}{RT} \cdot y_{A_2} = \frac{4.13 \times 0.040}{0.311 \times RT}$$

$L = 0.378$ cm

$A = 0.311$ cm

From equation (2)

$$D_{eff} = \frac{N_A \cdot RT \cdot L}{P(y_{A_1} - y_{A_2})} = \frac{4.13 \times 0.04 \times 0.378}{0.664 \times 0.96 \times 0.311} = 0.317\ cm^2/sec$$

The value of Q was calibrated at P = 1 atm.

B. The calculation of K_{eff} from flow measurement.

Molecular Sieve 4A

$P = 2.51$ atm

$Q \cdot P = 0.129\ (\frac{cm^3}{sec})$ (atm)

$\Delta P = 0.1056$ atm

$L = 0.378$ cm

$A = 0.311\ cm^2$

From equation (16)

$$K_{eff} = \frac{Q \cdot P \cdot L}{\Delta P \cdot A} = \frac{0.129 \times 0.378}{0.1056 \times 0.311} = 1.49 \text{ cm}^2/\text{sec}$$

The value of Q was calibrated at P = 1 atm.

C. The calculation of D_{eff} from mercury penetration data

Molecular Sieve 4A

$$\varepsilon_a = 0.42$$

$$\varepsilon_i = 0.27$$

$$\bar{v} = 1.78 \times 10^5 \text{ cm/sec}$$

$$\bar{r}_a = 5750 \text{ Å}$$

$$\bar{r}_i = 4 \text{ Å}$$

$$\bar{D}_{K_a} = \frac{2}{3} \bar{r}_a \bar{v} = 6.82$$

$$\bar{D}_{K_i} = \frac{2}{3} \bar{r}_i \bar{v} = 4.75 \times 10^{-3}$$

$$\alpha = 1 - \frac{M_B}{M_A} = 1 - \left(\frac{2}{28}\right)^{1/2} = 0.733$$

$$y_{A_2} = 0.0565$$

$$P = 6.23 \text{ atm}$$

$$D_{AB} = \frac{0.76}{6.23} = 0.122 \text{ cm}^2/\text{sec}$$

From equation (12)

$$D_{eff} = D_{AB} (a + i + S)$$

a = macropore contribution = 0.302

i = micropore contribution = 0.0278

S = series contribution = 0.00768

$$D_{eff} = 0.122 (0.302 + 0.0278 + 0.00768)$$

$$= 0.03812 \text{ cm}^2/\text{sec}$$

D. The calculation of K_{eff} from mercury penetration data.

Molecular Sieve 4A

$\varepsilon_a = 0.42$

$\bar{r}_a = 5750$ Å

$\bar{v} = 4.74 \times 10^4$ cm/sec (for N_2 at 25° C)

$\eta = 1.8 \times 10^{-4} \frac{\text{(dynes)(sec)}}{\text{cm}^2}$

$\varphi = 1.013 \times 10^6 \frac{\text{(dynes)(sec)}}{\text{(atm)(cm}^2\text{)}}$

P = 2.51 atm

From equations (23) and (28)

$$K_{eff} = \frac{2}{3} \bar{r} \bar{v} \varepsilon_a^2 + \frac{P \bar{r}^2}{8 \eta} \cdot \varphi \cdot \varepsilon_a^2$$

$$\frac{2}{3} \cdot \bar{r}\,\bar{v} \cdot \varepsilon_a^2 = 0.32 \text{ cm}^2/\text{sec}$$

$$\frac{P \cdot \bar{r}^2}{8\eta} \cdot \varphi \cdot \varepsilon_a^2 = 1.03 \text{ cm}^2/\text{sec}$$

$$K_{eff} = 0.32 + 1.03 = 1.35 \text{ cm}^2/\text{sec}$$

E. The calculation of ε and $\bar{r}$ from mercury penetration data

Molybdena Alumina Catalyst

From the pore size distribution plots ε vs. $\bar{r}$ (Fig. 3)

$$\varepsilon_a = 0.1585$$

$$\varepsilon_i = 0.461 - 0.1585 = 0.3025$$

$$\bar{r}_a = \frac{\int_0^{\varepsilon_a} r\,d\varepsilon}{\varepsilon_a} = \frac{\int_0^{0.1585} r\,d\varepsilon}{0.1585}$$

by graphical integration, $\int_0^{0.1585} r\,d\varepsilon = 222$

$$\bar{r}_a = \frac{222}{0.1585} = 1400 \text{ Å}$$

From the pore size distribution plots $\frac{\Delta\varepsilon}{\Delta \log r}$ vs. r (Fig. 6)

$$r_i = 44 \text{ Å}$$

F. The calculation of D_{eff} from κ_{eff}

Nickel Catalyst

From the plot of κ_{eff} vs. P

Slope = 0.190

Intercept = 0.177

$$\bar{r} = \frac{16\,\eta\,\bar{v}\,\text{slope}}{3\,\varphi\,\text{Intercept}} \times 10^{8} = 4830$$

$$\varepsilon x = \frac{9\,\varphi\,(\text{Intercept})^{2}}{32\,\eta\,\bar{v}^{2}\,(\text{Slope})} = 0.1162$$

$$\bar{D}_{\kappa_a} = \frac{2}{3}\,\bar{r}_a\,\bar{v} = 5.735$$

P = 3.4 atm

$$D_{AB} = \frac{0.76}{3.4} = 0.223$$

From equation (11)

$$D_{eff} = D_{AB} \cdot a$$

a = macropore contribution = 0.1983

$$D_{eff} = 0.223 \times 0.1983 = 0.0442$$